CHAPTER

16

Dissolved organic carbon in the South China Sea

Minhan Dai, Xiaolin Li, Yao Zhang, Feifei Meng, and Zhixuan Wang

State Key Laboratory of Marine Environmental Science, College of Ocean and Earth Sciences, Xiamen University, Xiamen, China

OUTLINE

List of acronyms

AOA	ammonia-oxidizing archaea
AOU	apparent oxygen utilization
BDOC	biodegradable dissolved organic carbon
BP	bacterial production
BR	bacterial respiration
CR	community respiration
DIC	dissolved inorganic carbon
DIN	dissolved inorganic nitrogen
DIP	dissolved inorganic phosphorus
DOC	dissolved organic carbon
DON	dissolved organic nitrogen
ECS	East China Sea
FDOM	fluorescent dissolved organic matter
GPP	gross primary production
KC	Kuroshio Current
LOC	labile organic carbon
NOB	nitrite-oxidizing bacteria
NPIW	North Pacific Intermediate Water
NPP	net primary production
NSCS	northern SCS
PCD	prokaryotic carbon demand
PGE	prokaryotic growth efficiency
POC	particulate organic carbon
RDOC	refractory DOC
ROC	recalcitrant organic carbon
ROMS	Regional Ocean Modeling System
SCS	South China Sea
SEATS	Southeast Asian Time-series Study
SLDOC	semilabile DOC
SRDOC	semirefractory DOC
SSCS	southern SCS
wNP	western North Pacific Ocean
WPS	West Philippine Sea

16.1 Introduction

Ocean margins play a disproportionately important role in the global carbon budget relative to their size; however, the mechanistic understanding required to simulate and predict future changes in their carbon cycle remains insufficient (Dai et al., 2022 and references therein). This deficit in understanding exists because carbon dynamics in ocean margins are associated with large spatiotemporal variations in carbon fluxes modulated by a combination of complex physical and biogeochemical processes. Moreover, ocean margins are in a transitional region between land and the open ocean and are thus extrinsically modulated by both riverine inputs and exchange with the open ocean. They are thus characterized by higher spatiotemporal gradients in almost all chemical and biotic parameters than in the open ocean (Dai et al., 2013, 2022). Anthropogenic activities such as land-use modification, waterway impoundment, nutrient inputs, and wetland degradation add even greater complexity and uncertainty (e.g., Dai et al., 2023; Bauer et al., 2013). The factors mentioned above increase the difficulty of undertaking biogeochemical studies in ocean margins.

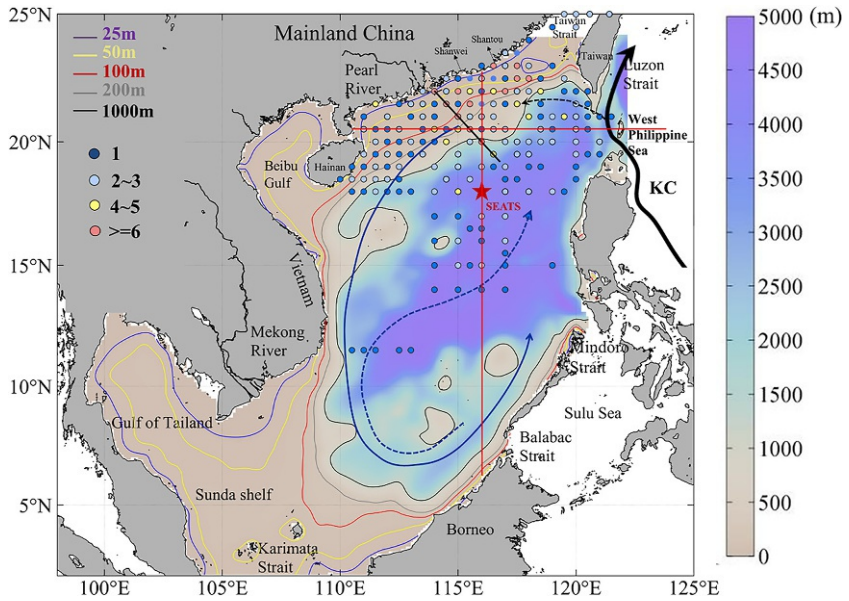

FIG. 16.1 Map of the South China Sea (SCS) showing bathymetry (isobaths at 25, 50, 100, 200, and 1000 m indicated by contour lines) and basin-scale surface circulation patterns (cyclonic in summer *(blue solid line)* and anticyclonic in winter *(blue dashed line)*). The *black solid line* indicates the path of the Kuroshio mainstream. An intrusion of Kuroshio Current (KC) waters into the SCS via the Luzon Strait is shown by the *black dashed line*. The observational stations used for DOC reconstruction are indicated by dots superimposed by observation frequency. DOC distributions along transects *(red lines)* are discussed in Section 16.2.1. A *black line* extending from the Pearl River estuary to the northern basin denotes Section 16.2.1, which has been frequently occupied. The seasonal variations in DOC in Section 16.2.1 are described in Section 16.2.2. The location of the Southeast Asian Time-series Study (SEATS) station (116°E, 18°N) is shown by the red star.

The South China Sea (SCS, Fig. 16.1) is the largest marginal sea of the North Pacific Ocean. It is a complex ocean margin bounded in the north by the shores of South China; in the west by the Indochinese Peninsula; in the east by the Taiwan Island and the northwestern by Philippines; and in the south by Borneo, eastern Sumatra, and the Bangka Belitung Islands. The SCS encompasses an area of approximately 3,500,000 km^2, including a large northeast-southwest oriented abyssal basin with a maximum depth reaching more than 5560 m, and extensive continental shelves to the northwest and south covering 48% of the SCS with water depths shallower than 200 m. The abyssal basin underlies 16% of the SCS surface area, while the continental and island slopes occupy 36% (Zheng et al., 2020).

The waters of the SCS exchange with the West Philippine Sea (WPS) in the western North Pacific Ocean (wNP) via the Luzon Strait, the East China Sea (ECS) via the Taiwan Strait, the Java Sea via the Karimata Strait, and the Sulu Sea via the Mindoro and Balabac Straits. The Luzon Strait has the deepest sill (~ 2400 m) and is the only gateway for deep water from the adjacent wNP. The SCS is thus semienclosed, and the deeper part of the SCS is confined to a bowlshaped trench, suggesting that the SCS is a completely isolated basin below 2400 m, with no direct water exchange with the surrounding oceans (Qu et al., 2006; Tian et al., 2009).

The SCS experiences the southwest monsoon from May to August and the northeast monsoon from October to March. The northeast monsoon is usually stronger than the southwest monsoon in terms of wind speed, but precipitation is higher during the southwest monsoon (Liu et al., 2010). The SCS is frequently impacted by typhoons (~10 annually on average), with most typhoons occurring to the north of 10°N from May to October. Typhoons typically bring a considerable amount of rain to the SCS, such that precipitation is greatest during the southwest monsoon period.

The SCS features a seasonally influenced, layered circulation pattern (Gan et al., 2016). In the upper layer (<750 m), the intrusion of Kuroshio water, a major western ocean boundary current, and a positive wind stress curl result in an extensive cyclonic circulation (Gan et al., 2016; Liu and Gan, 2017). Here, the surface currents are driven to a significant extent by the monsoons, with a cyclonic gyre appearing during the northeast monsoon and an anticyclonic gyre appearing during the southwest monsoon (Fig. 16.1). These basin scale surface currents effectively isolate the SCS basin from terrestrial inputs, so a wide area of the SCS basin is oligotrophic. In the deeper layers (>1500 m), the intrusive, denser western Pacific water passes through the Luzon Strait and cascades downwards into the enclosed SCS deep basin. It then flows southwestward along the slope, where an extensive eddy-like cyclonic circulation pattern induces complex vertical flow (Gan et al., 2016; Liu and Gan, 2017). Given the fast replenishment, with a residence time of less than 30 years in the deep SCS, the deep water must return to the upper layer through strong diapycnal mixing (Gan et al., 2016; Liu and Gan, 2017; Qu et al., 2006). This upwelled deep water renews the intermediate water (750–1500 m) layer that circulates anticyclonically, with the longest residence time (~42 years) in the southern SCS (SSCS) (Liu and Gan, 2017). Strong vertical flows of denser intermediate water in the northern SCS (NSCS) and over the slope regions, where upwelling is a prominent feature (Liu and Gan, 2017), are often observable. Simulations of SCS circulation with the Regional Ocean Modeling System (ROMS) reveal that the inwards-outwards-inwards transport through the Luzon Strait has a layer-integrated net input to the SCS of 5.9 Sv (10^6 m^3 s^{-1}) in the upper 750 m. The transport is relatively small in the middle (750–1500 m, −1.4 Sv) and deep layers (>1500 m, 0.9 Sv) (Gan et al., 2016).

The SCS receives abundant terrestrial inputs from riverine discharges. The Mekong River, the world's 10th largest river with an annual water discharge of 475 km^3, is the largest river emptying into the SCS (Adamson et al., 2009). The Mekong River plume can travel over a thousand kilometers, impacting both the hydrology and biogeochemistry of the western SCS (Chen et al., 2010). The Pearl River, with an annual freshwater discharge of 285 km^3, is the 2nd largest river discharged into the SCS, entering from southern China (Cao et al., 2011; Dai et al., 2013). The total runoff to the SCS is estimated to be 3282 km^3 $year^{-1}$ (Syvitski et al., 2005). This significant freshwater input makes the SCS one of the largest recipients of riverine runoff, with 9.3 km^3 per year per 10,000 km^2 of sea surface area. This rate surpasses that of the Arctic Ocean, which, as the largest ocean basin receiving river runoff, has an input of 4.2 km^3 per year per 10,000 km^2 of sea surface area (Stadnyk et al., 2021).

The SCS features extensive shelves in both the north and south. The NSCS shelf stretches from the northwest to the southeast of mainland China and from the coast to approximately the 200 m isobath (Fig. 16.1). It includes the Beibu Gulf, a semienclosed shallow bay with a surface area of 126,250 km^2. The SSCS shelf mainly includes the Sunda Shelf, which is the second-largest submerged extension of a continental margin in the world, with an extremely

low gradient (Hanebuth et al., 2011). The Sunda Shelf has a surface area of $1.85 \times 10^6\,km^2$ and is 100 m deep in the center, compared to the adjacent Gulf of Thailand, which is approximately 70 m deep. These shelf systems share many common coastal current features, as well as seasonal coastal upwellings and river plumes that are strongly influenced by local circulation, topography, and tides (Dai et al., 2014; Hu and Wang, 2016; Zheng et al., 2020). These hydrographic features cumulatively have important impacts on the regional biogeochemistry of the SCS, including that of DOC.

The basin area of the SCS is strongly stratified and depleted in nutrients in surface waters; thus, primary productivity remains very low (Du et al., 2013; Tseng et al., 2005; Wu et al., 2003; Zhu et al., 2021). Cyclonic eddies and monsoonal wind-induced mixing affect the rates of deep nutrient supply to the euphotic zone through upwelling and mixing (Du et al., 2017; Lu et al., 2020; Xiu et al., 2018). Additionally, seasonality of the Kuroshio intrusion, which carries oligotrophic water, significantly influences nutrient distributions and inventories in the SCS (Du et al., 2013). These vertical and horizontal processes further regulate primary and export productivity as well as nutrient regeneration (Lu et al., 2020). In winter, increased wind stress stimulates photosynthesis through strong mixing that entrains the nutrient-rich subsurface water to the upper layer; in summer, the upper water column is highly stratified, resulting in reduced biological productivity. Du et al. (2013) determined that the degree of the Kuroshio intrusion into the SCS also significantly impacts the upper SCS nutrient inventory.

As a project in the Joint Global Ocean Flux Study (JGOFS), the Southeast Asian Time-series Study (SEATS) station was established at 18.0°N and 116.0°E in the NSCS basin in 1999. Since then, the SEATS station has been studied at roughly seasonal intervals to investigate the biogeochemical cycling of carbon, nutrients, and relevant bioelements over intra-annual to decadal timescales (Wong et al., 2007). The location is characterized by high surface temperature showing little seasonality, oligotrophic surface waters, and persistent stratification with a thin mixed layer. However, well-defined seasonal patterns were observed in the carbon cycle, nutrient dynamics, phytoplankton community structure, and biological productivity (Chou et al., 2006, 2007; Tseng et al., 2007; Sheu et al., 2010; Kao et al., 2012; Liu et al., 2013; Du et al., 2017; Zhou et al., 2020). This time-series effort improved our understanding of SCS basin biogeochemistry at different timescales (Wong et al., 2007; Liu et al., 2013, 2018; Zhou et al., 2020; Dai et al., 2022).

The biogeochemistry of the SCS shelf is modulated by river plumes, coastal upwelling, and coastal currents (Cao et al., 2011; Han et al., 2012; Dai et al., 2014; Zhao et al., 2021) and is thus seasonally variable. Taking the NSCS as an example, the upslope advection of subsurface waters intensifies the cross-shelf advection off Shanwei and is then subsequently transported northeastward by the upwelling coastal current and outcropped at the lee of the coastal cape off Shantou (Han et al., 2012). The Pearl River plume interacts with upwelling and wind-driven currents near the surface, whereas it becomes advected eastwards (Zhao et al., 2021). Along with these physical processes, organic matter appears to be remineralized, with dissolved inorganic carbon (DIC) and nutrients regenerated along with the upslope advection of subsurface waters toward Shanwei. On the inner shelf along the upwelling coastal current from Shanwei to Shantou, there is a northwards enhancement of DIC and nutrient consumption rates, although regeneration and consumption of DIC and nutrients (notably for $Si(OH)_4$) coexisted. Dissolved inorganic nitrogen (DIN) and phosphorus (DIP) consumption follow the

Redfield stoichiometry. In the plume areas, the net consumption of nutrients and DIC is obvious, with an apparent non-Redfield DIN:DIP uptake ratio (Han et al., 2012).

Taken together, observational and numerical modeling studies have made considerable progress in understanding the biogeochemistry of the SCS under the modulation of physical dynamics (e.g., Wong et al., 2007; Dai et al., 2013; Du et al., 2017, 2020). There are three distinct biogeochemical provinces in the SCS: the shelf and gulf systems under strong influences of terrestrial inputs; the area of the deep basin, which is permanently stratified as an open-ocean regime; and the transitional zone in the northeastern SCS exhibiting vigorous water mass and material exchanges with the Kuroshio. While shelf systems, such as the NSCS, are characterized as river-dominated ocean margins (RiOMar), both the SCS basin and transitional zones are open ocean-dominated margins (OceMar) (Dai et al., 2013, 2022; Cao et al., 2020).

This chapter presents the DOC biogeochemistry of the SCS based on data collected during the past twenty years (e.g., Callahan et al., 2004; Dai et al., 2009; He et al., 2010; Wu et al., 2015; Meng et al., 2017; Ding et al., 2020, 2022; Jiang et al., 2023; Li et al., 2018, 2021). The application of numerical models has also emerged as a powerful tool for reconstructing high-resolution DOC distributions and quantitatively assessing the exchange of DOC with adjacent oceans and seas (Gan et al., 2016; Lu et al., 2018; Ma et al., 2021). While we demonstrate the concept of the SCS as a mini ocean in general, we also discuss the important features of DOC in the biogeochemical provinces of the SCS.

16.2 DOC distribution in the South China Sea

16.2.1 Overview

Surface DOC concentrations are higher on the NSCS shelf than over the basin. DOC concentrations in the SCS are generally lower than in the wNP in the upper layers (5 and 100 m, as seen in Fig. 16.2A and B). According to the zonal transect, the thickest high-DOC surface layer is located in the wNP, while the shallow DOC contours tend to shoal toward the west (Fig. 16.3B). In the upper 1000 m of the vertical gradient, DOC drops from 75 to 45 mol L^{-1} (Figs. 16.2 and 16.3). Below 2000 m, DOC concentrations are homogeneous in the SCS, comparable to that at 2000 m in the wNP (Figs. 16.2D and 16.3).

16.2.2 Spatial and temporal variations

16.2.2.1 Northern South China Sea shelf

On the NSCS shelf, where the water depth is shallower than 200 m, the surface distributions of DOC exhibit considerable regional and seasonal variability largely corresponding to that of the sea surface salinity (Fig. 16.4). Throughout all seasons, surface DOC is often higher in the nearshore than in the offshore regions. When examined seasonally, they are on average higher in summer and autumn than in spring and winter. The highest values of DOC observed (up to 117 μmol L^{-1}) were in the river plume, which is defined as buoyant water with sea surface salinity <33.0 in the top 20 m. DOC and salinity generally display a

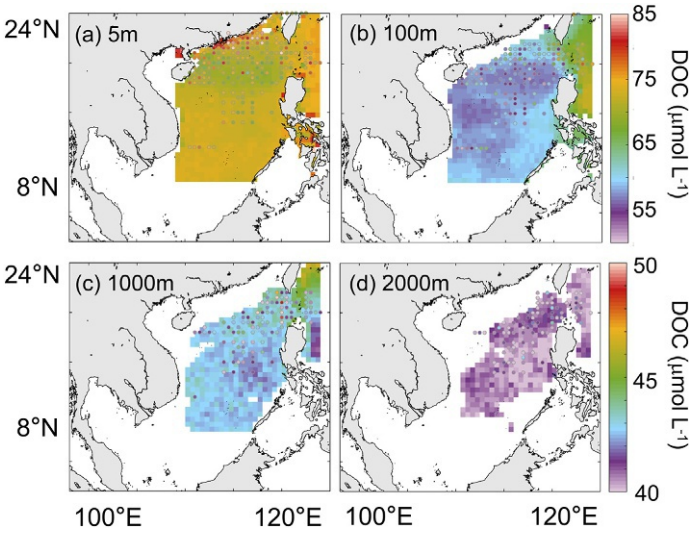

FIG. 16.2 Spatial distributions of DOC concentrations at (A) 5 m, (B) 100 m, (C) 1000 m, and (D) 2000 m water depths in the South China Sea, primarily based on reconstructed DOC. The observed DOC data are also shown in points. The reconstruction is based on the large observational dataset of DOC concentrations collected from 2005 to 2018 (e.g., Dai et al., 2009; Wu et al., 2015; Meng et al., 2017; Ding et al., 2020) using a machine learning algorithm to increase its spatial and temporal coverage in the SCS (Fig. 16.1). The data input to the reconstructed algorithm includes multiobservation Global Ocean 3D temperature, salinity data (downloaded from https://data.marine.copernicus.eu/product/), remote sensing-derived sea surface chlorophyll data (download from https://oceancolor.gsfc.nasa.gov/l3/), the total organic carbon (TOC) accumulation rate (calculated according to Kao et al., 2006), time labels (seasonal), and depth information. Note that all these data used in machine learning have been interpolated on the same grid, and the bias between in situ DOC data and the reconstructed data is approximately 2 μmol L^{-1}.

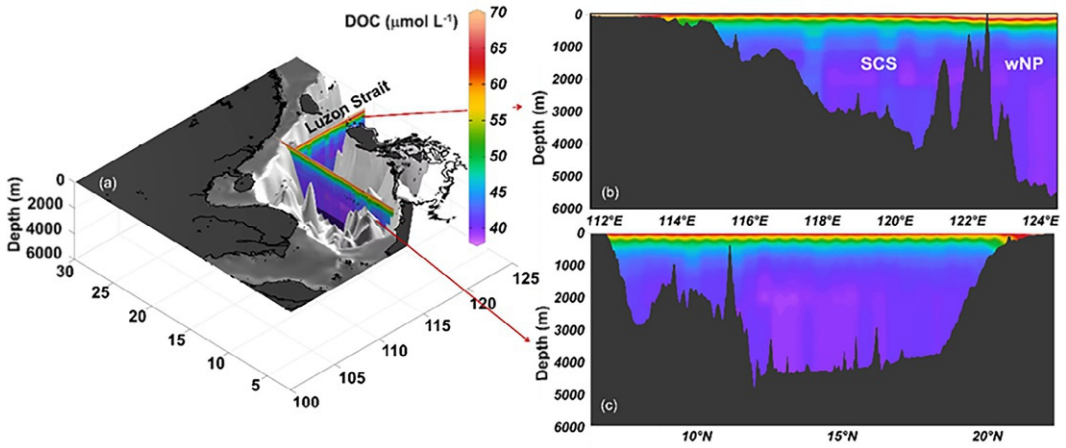

FIG. 16.3 South China Sea topography (A) and vertical profiles of climatological reconstruction of DOC on a zonal section along 20°N (B) and (C) the meridional transect along 116°E (locations shown in Fig. 16.1).

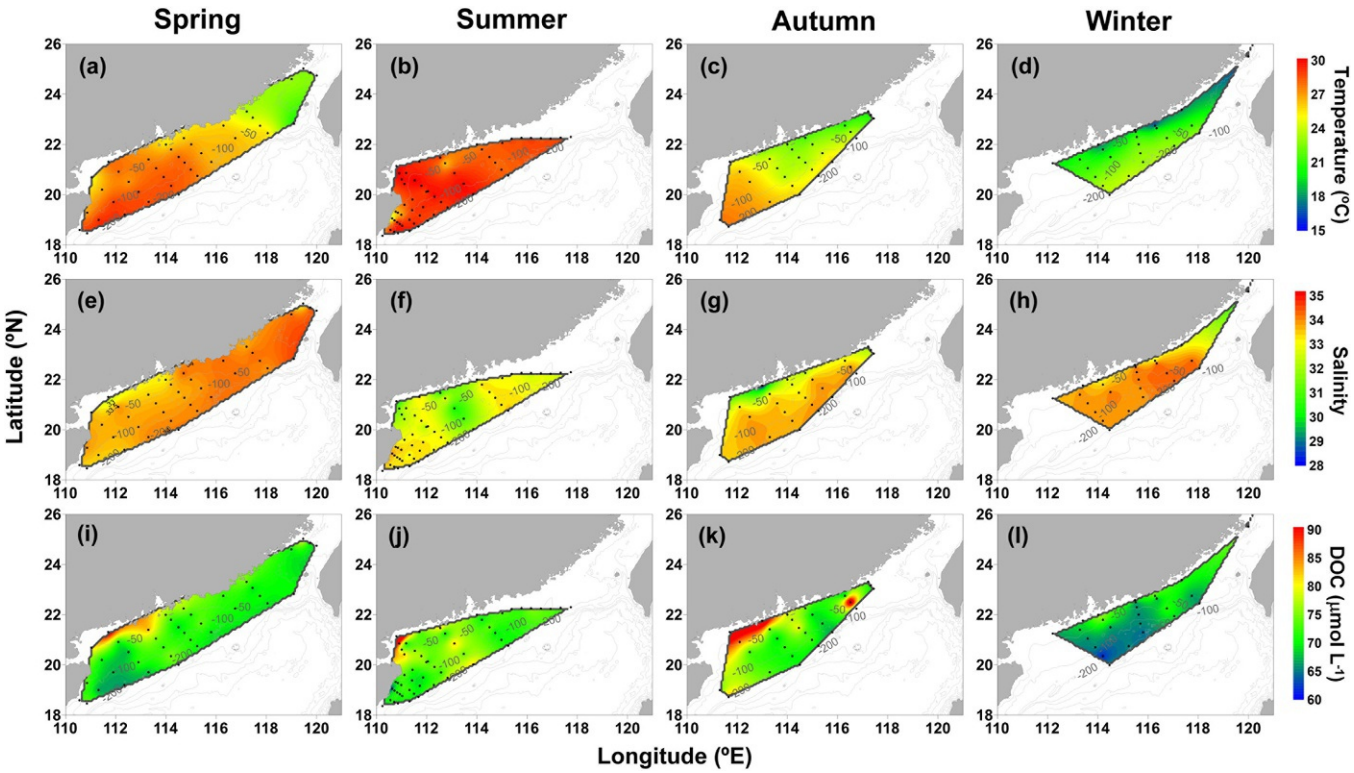

FIG. 16.4 Surface distributions of (top) temperature, (middle) salinity, and (bottom) DOC on the northern South China Sea shelf during spring, summer, autumn, and winter. (A) Spring: temperature, (B) summer: temperature, (C) autumn: temperature, (D) winter: temperature, (E) spring: salinity, (F) summer: salinity, (G) autumn: salinity, (H) winter: salinity, (I) spring: DOC, (J) summer: DOC, (K) autumn: DOC, (L) winter: DOC. *Black dots* represent sampling stations. *Reprinted from Meng et al. (2017), with permission from John Wiley and Sons.*

negative correlation in the plume water with lower DOC concentrations at higher salinities, suggesting the overall dilution of riverine DOC by seawater. The influence of plume water is more distinguishable in summer and autumn (Fig. 16.4).

Vertical section distributions of DOC generally associate with those of temperature and salinity on the shelf (Fig. 16.5). The waters are largely stratified in spring and summer, being characterized by decreasing DOC and temperature and increasing salinity from surface to bottom. DOC at each sampling depth is lower in the subsurface layer in summer, corresponding to lower temperature and higher salinity (Fig. 16.5B), likely a result of the uplift of DOC-poor subsurface waters during intensified upwelling on the shelf (Wu et al., 2017). The small vertical gradients of DOC in autumn (i.e., top to bottom) disappeared in winter when the shelf waters were thoroughly mixed (Fig. 16.5C and D). DOC values are overall higher throughout the water column in autumn than during the other seasons (Fig. 16.5C), as a result, the DOC inventory is highest in autumn, probably resulting from DOC accumulation in the water column during the seasonal transition of hydrographic conditions from stable stratification to dynamic mixing (Meng et al., 2017).

16.2.2.2 Slope and basin

The surface distribution of temperature shows a typical seasonal pattern with higher values in summer and lower values in winter (Fig. 16.6). Surface salinity shows a north-to-south gradient with higher values in the northern SCS, particularly off the Luzon Strait. The enhanced Kuroshio intrusion onto the NSCS and attenuated evaporation in the SSCS make this gradient more pronounced in winter (Fig. 16.6).

The DOC distribution pattern in the SCS is generally consistent with that of temperature and salinity, generally reflective of the influences of water mass mixing and, to a lesser extent, DOC production. In summer, DOC concentrations display a northwest-to-southeast gradient at 50, 70, and 100 m (Fig. 16.6). Lower values are found in the northwestern SCS off Hainan and Vietnam, attributed to the upwelling of low DOC subsurface waters, manifested by lower temperatures and higher salinities observed in this area (Hu and Wang, 2016). In winter, relatively lower surface DOC concentrations are observed in the NSCS basin, attributed to the deepening of the surface mixed layer depth (Du et al., 2021). Decreased diapycnal mixing in the upper SCS, from the Luzon Strait to the southwestern basin, is responsible for the higher DOC concentrations observed in the southwestern basin at 5 and 50 m (Fig. 16.6).

16.2.2.3 SEATS station in the basin

As described in the preceding sections, temperature variations at SEATS in the upper 100 m of the water column also show a seasonal pattern with winter minima and summer maxima (Fig. 16.7B). The seasonal variation in surface chlorophyll is similarly well defined, showing high concentrations in winter but low concentrations in summer (Fig. 16.7C), consistent with previous research (Liu et al., 2013; Xiu et al., 2019). Below 100 m, the seasonal cycle of temperature is less pronounced.

While DOC concentrations at SEATS generally decrease with increasing water depth (Fig. 16.7A), their temporal variability is more complex. Seasonal and interannual variations in vertical and lateral water mass mixing as well as primary production have a significant impact on the temporal pattern of upper water column DOC. Winter overturn and mixing of the water column were both causes of DOC reductions and nutrient entrainment in the

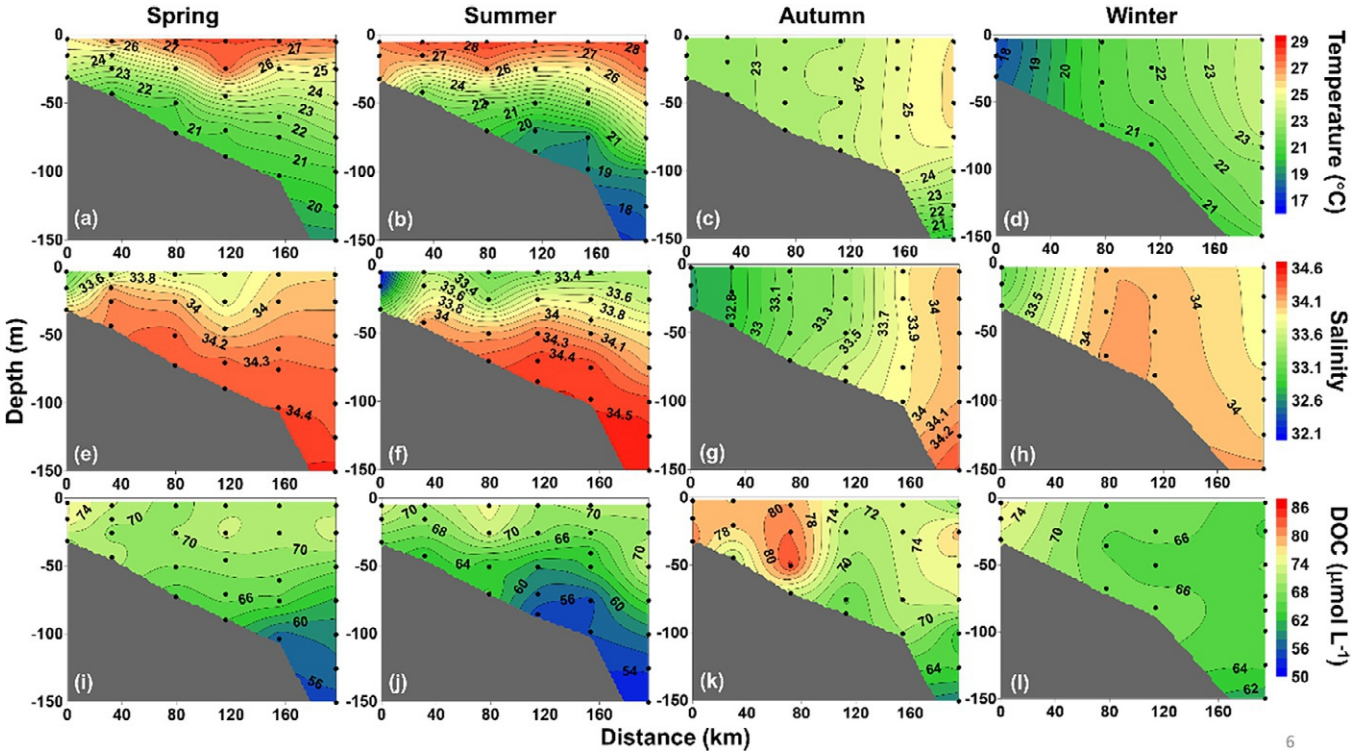

FIG. 16.5 Distributions of temperature, salinity, and DOC along transect A (location shown in Fig. 16.1) across the northern South China Sea shelf. (A) Spring: temperature, (B) summer: temperature, (C) autumn: temperature, (D) winter: temperature, (E) spring: salinity, (F) summer: salinity, (G) autumn: salinity, (H) winter: salinity, (I) spring: DOC, (J) summer: DOC, (K) autumn: DOC, (L) winter: DOC. *Black dots* represent sampling depth. *Redrawn from Meng et al. (2017), with permission from John Wiley and Sons.*

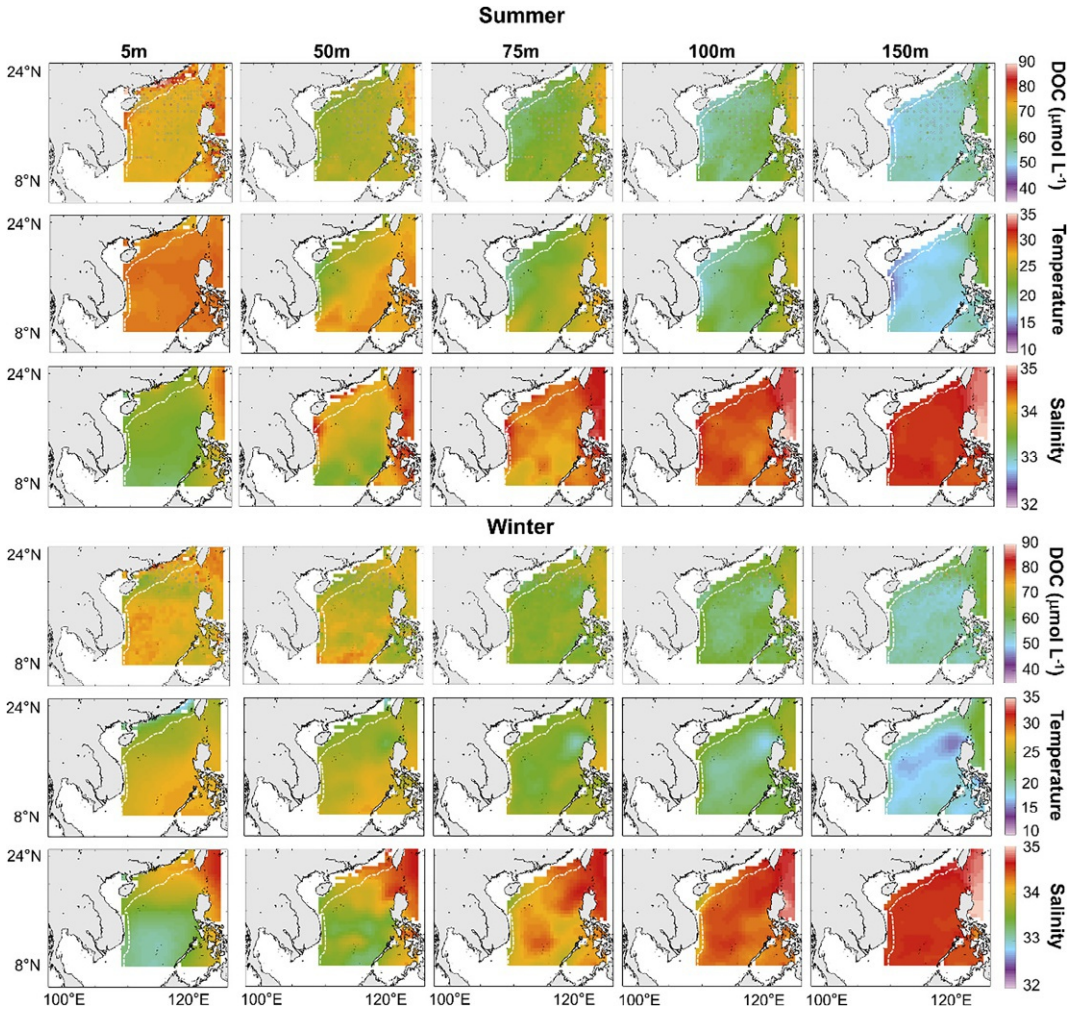

FIG. 16.6 Seasonal distributions of reconstructed DOC concentrations, temperature, and salinity at 5 depths (5, 50, 75, 100, 150 m) in the South China Sea and adjacent western North Pacific Ocean. The observed DOC data are also shown in points. The isobath at 200 m is indicated by the *white dashed line*.

upper layer (Hansell and Carlson, 2001). As a result, DOC production may surpass DOC consumption, which could lead to an accumulation of DOC over the subsequent water-stratified spring and summer with shallower mixed layer depths (Fig. 16.7A). The seasonally accumulated surface DOC, itself resistant to microbial degradation, is exported out of the euphotic zone during the annual convective mixing in winter (December–February) (Fig. 16.7A). DOC unused by the surface water bacterioplankton assemblage may become bioavailable once exported to the mesopelagic zone (Carlson et al., 1994, 2004; Hansell and Carlson, 2001).

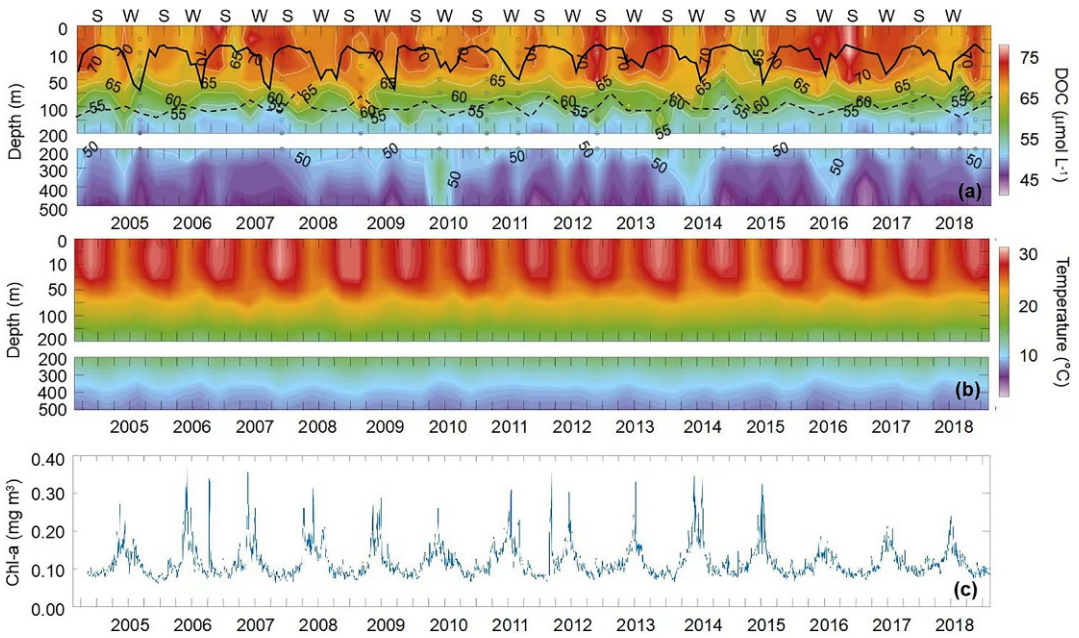

FIG. 16.7 Time-series of reconstructed DOC concentrations (A), temperature (B) in the upper 500 m, and surface chlorophyll (C) at the SEATS station. The observed DOC data are shown in points in (A). To better represent the details of (A) and (B), a nonlinear depth setting is applied for depths shallower than 200 m. The *black solid* and *dashed lines* in (A) represent the depths of the mixed layer and euphotic zone, respectively. "S" and "W" represent summer and winter, respectively. Euphotic zone depth data were provided by Dr. Xiaolong Yu (Xiamen University). Remote sensing-derived sea surface chlorophyll data were provided by the ACRI-ST company (Sophia Antipolis, France) based on the Copernicus-GlobColor processor and downloaded from https://data.marine.copernicus.eu/product/OCEANCOLOUR_GLO_BGC_L4_MY_009_104/. Mixed layer depth data were downloaded from https://scihub.copernicus.eu/.

16.2.3 Comparison of DOC distributions between the SCS and the wNP

As shown in the temperature-salinity (T-S) diagram (Fig. 16.8), the hydrographic properties of the SCS are closely related to, but distinctly different from, the wNP water. The lowest surface salinity is in the SSCS, attributable to large riverine inputs and basin-wide net precipitation in the SCS interior (Wyrtki, 1961). Intensive upwelling and vertical mixing in the SCS interior reduce this extreme signal (Cao and Dai (2011) and references therein), resulting in a less curved pattern of T-S distributions in the SCS relative to the wNP (Fig. 16.8). Waters collected at most sampling stations in the NSCS are mixtures of end-members SSCS and wNP.

In the SCS basin, vertical profiles of DOC generally show a pattern of high concentrations in the upper mixed layer (65–74 μmol L^{-1}), with sharp decline to ~46 μmol L^{-1} by 500 m (Fig. 16.9A). There is a significant negative correlation between DOC and apparent oxygen utilization (AOU) in the depth interval where DOC concentrations sharply decline, from the

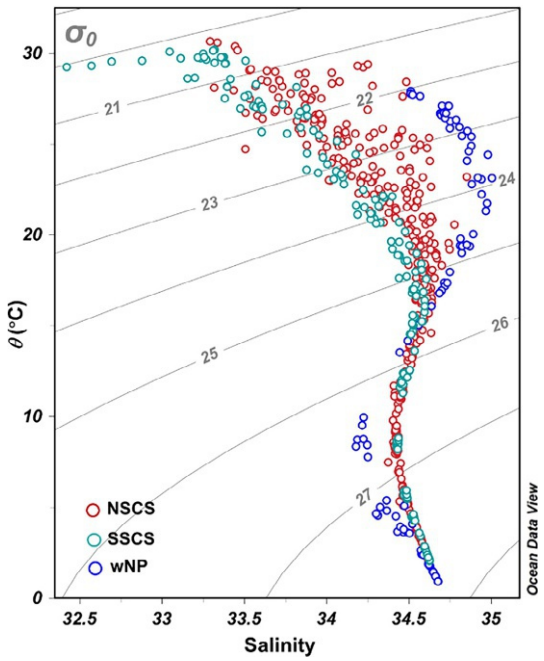

FIG. 16.8 Relationships of potential temperature (θ) and salinity in the SCS and wNP. NSCS: northern South China Sea; SSCS: southern South China Sea; wNP: western North Pacific Ocean. Data in the NSCS are from Dai et al. (2009), Wu et al. (2015), and Ding et al. (2020). Data in the SSCS were collected in May 2014. Hydrological data for the reference stations in the wNP (126°E, 17°58′N; 128°6′E, 17°57′N; 130°E, 17°59′N; 129°53′E, 19°55′N, 128°E, 20°N, 125°59′E, 20°2′N, 124°57′E, 19°58′N) were collected in November 2014.

bottom of the mixed layer to 500 m [DOC $= -(0.1031 \pm 0.0028)$ AOU $+ (62.8071 \pm 0.2908)$, $r^2 = 0.8135$, $n = 309$] (Fig. 16.10). The correlation suggests that DOC consumption is closely linked to the generation of AOU through remineralization or the mixing of various water masses (Pan et al., 2014). Strengthened diapycnal mixing in the NSCS (both in the upper layer and the mid-to-deep layers) (Liu and Gan, 2017; Wang et al., 2019) diminishes the vertical DOC gradient, resulting in statistically lower values in the upper 100 m of the water column and higher values below, relative to the gradient in the SSCS (Fig. 16.9C).

Compared to the wNP, DOC in the upper 1000 m of the SCS is generally lower (Fig. 16.9A). Such a deficit in DOC is partly caused by rapid mixing with DOC-depleted deeper water and enhanced biodegradation (details are discussed in Section 16.3) (Qu et al., 2006). Additional causes include the relatively higher bacterial production in the NSCS than in the wNP at the surface (Shiah et al., 1998; Wu et al., 2015). The DOC concentration in the SCS below 2000 m has a narrow range of $39.7 \pm 1.2\,\mu mol\,L^{-1}$ ($n = 45$), comparable to North Pacific Intermediate Water (NPIW, DOC $= 38.7 \pm 0.7\,\mu mol\,kg^{-1}$, Hansell et al., 2002). Such an identical DOC concentration confirms a rapid deepwater exchange between the two basins, also indicated based on the insignificant difference between the SCS and the wNP in Δ^{14}C-DIC below 1500 m (Broecker et al., 1986). The most important difference between the DOC profiles of the SCS and the wNP is that there is additional DOC accumulated in the SCS below 1000 m at potential densities between 27.3 and 27.7, as evident on the potential density (σ_θ) versus DOC plot (Fig. 16.9B).

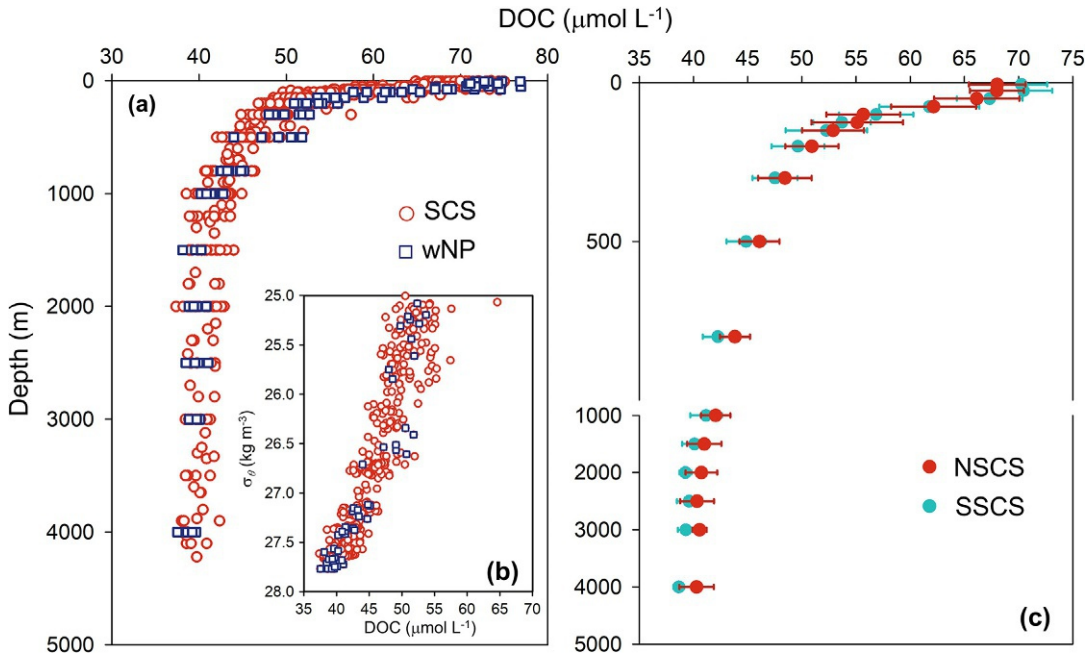

FIG. 16.9 (A) Depth profiles of DOC in the SCS and wNP. (B) Potential density (σ_θ) versus DOC concentration for all corresponding samples in (A). (C) Depth profiles of averaged DOC in the SCS. Standard deviations are shown as error bars. Data in the NSCS are from Dai et al. (2009), Wu et al. (2015), and Ding et al. (2020). Data in the SSCS were collected in May 2014. Hydrological data for the reference stations in the wNP (126°E, 17°58′N; 128°6′E, 17°57′N; 130°E, 17°59′N; 129°53′E, 19°55′N, 128°E, 20°N, 125°59′E, 20°2′N, 124°57′E, 19°58′N) were collected in November 2014.

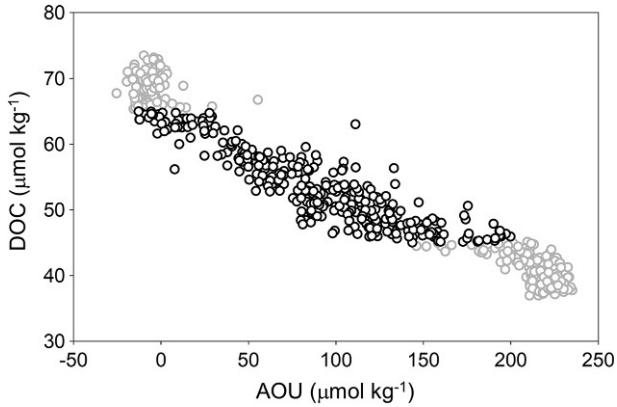

FIG. 16.10 Scatterplot of DOC versus AOU in the SCS. The *black circles* denote data points collected in the depth interval where DOC concentrations sharply decline. The *gray circles* denote all the data collected in the water column.

16.3 DOC production, transformation, and consumption

16.3.1 Influences of river plumes, coastal upwelling, and seasonal coastal currents along the NSCS shelf

River inputs and coastal upwelling are two important processes that shape the distribution of DOC in the coastal ocean. The Pearl River transports significant amounts of terrestrial and riverine organic matter into the NSCS (Dai et al., 2014). The input of organic matter by the river plume increases coastal DOC concentrations, while the upwelling of low-DOC water decreases DOC concentrations. Furthermore, elevated nutrient levels, compared to those found in the oligotrophic outer shelf, are typically observed in the nearshore area due to the upwelling (Han et al., 2012). Therefore nutrients provided by river plumes and coastal upwelling enhance primary production by phytoplankton, resulting in elevated POC concentrations and increased release of DOC (Song et al., 2012; Wu et al., 2017). Using a three-end-member mixing model (river plume, surface water, and subsurface water), the mixed-layer-integrated net DOC production rate was estimated to be $11.5 \pm 6.9\,\text{mmol C}\,\text{m}^{-2}\,\text{day}^{-1}$ in the upwelling zone and $7.1 \pm 7.0\,\text{mmol C}\,\text{m}^{-2}\,\text{day}^{-1}$ in the plume water (Wu et al., 2017). These results suggest that there is comparable in situ DOC production during both processes. DOC freshly produced from phytoplankton is highly bioavailable and readily utilized by bacteria (Shen et al., 2012).

In addition, the distribution of DOC on the NSCS shelf is influenced by the along-shelf and intershelf transport processes via the seasonal coastal current, which flows southwestward in winter and northeastward in summer. In winter, the coastal current delivers DOC from the ECS to the NSCS through the Taiwan Strait. Based on the wintertime depth-integrated average DOC concentration in the water column of $67.7 \pm 0.6\,\mu\text{mol}\,\text{L}^{-1}$ in the Taiwan Strait and the average volume transport of 0.13 ± 0.09 Sv (Han et al., 2013), the total DOC transport has been estimated to be $(8.2 \pm 5.7) \times 10^{11}$ g C from December to February (Meng et al., 2017). Furthermore, the coastal current transports a significant amount of nutrients from the ECS into the NSCS, sustaining primary production therein. The new production stimulated by these nutrient inputs has been estimated at $(8.8 \pm 6.3) \times 10^{11}$ g C (Han et al., 2013). Assuming a value of 17% (Hansell and Carlson, 1998; see Chapter 17, Table 17.2) for the portion of new production accumulating as DOC, extra DOC via photosynthetic production in the coastal current can be estimated to be $(1.5 \pm 1.1) \times 10^{11}$ g C in winter. This value is approximately one order of magnitude higher than the DOC input of 3.1×10^{10} g C from the Pearl River (estimated based on a survey in January 2011; Meng et al. (2017)).

16.3.2 Impacts on the NSCS from the Kuroshio intrusion

Featuring high temperature, high salinity, and oligotrophy, the Kuroshio Current intrudes into the SCS mainly above 350 m (Qu et al., 2000; Tian et al., 2006; Furue et al., 2009) through the Luzon Strait, creating a unique environment where many biogeochemical reactions are promoted (e.g., Zhu et al. 2021; Fig. 16.1). Typically, the Kuroshio Current penetrates further into the SCS during winter and tends to transit the Luzon Strait in summer (Nan et al., 2015; Du et al., 2013). As a result, the influence of the Kuroshio intrusion on temperature, salinity, nutrients, circulation, and eddy generation in the SCS varies seasonally.

Due to the higher DOC concentrations in the wNP than in the SCS, the intrusion of Kuroshio water leads to an increase in DOC concentration and inventory in the upper 500 m of the NSCS (Wu et al., 2015). The lateral mixing of water masses induced by the intrusion of the Kuroshio Current can synergistically facilitate nonlocal bacterial inoculation and increase nutrient supplies to these bacteria, which may activate the remineralization of DOC, including both the local SCS DOC and the intruded wNP DOC. Approximately 10% of surface DOC can be remineralized due to enhanced biodegradation in the SCS, and approximately 8.6 Tg C year^{-1} can be transferred and potentially remineralized within the top 150 m across the Luzon Strait (Li et al., 2021). Notably, the rate of DOC degradation may be a unimodal function of the proportion of Kuroshio water. Bacterial abundance, production, and growth efficiency were maximal at approximately 60% Kuroshio water mixed by the intrusion of the Kuroshio Current (Huang et al., 2019).

Lateral mixing induced by the intrusion of the Kuroshio Current introduces allochthonous dissolved organic nitrogen (DON) to the NSCS. This addition can enhance ammonium regeneration by activating the remineralization of the DON (Xu et al., 2018; Zhu et al., 2021). The amount of nitrogen released by the remineralization of DON is approximately 1.2 Tg N year^{-1} in the surface water (Li et al., 2021). The ammonium produced through the remineralization of DON is subsequently utilized by plankton, including assimilation by phytoplankton and oxidation by nitrifiers (Xu et al., 2018), driving sequential responses of biogeochemical processes in the SCS. For example, studies along the Kuroshio intrusion route found that enhanced gross primary production and nitrate concentration are maximal at approximately 50% Kuroshio water, following the regenerated ammonium maximum at approximately 50%–60% Kuroshio water (Huang et al., 2019; Zhu et al., 2021; Fig. 16.11). However, little impact of the Kuroshio intrusion was found on bacterial and community respiration (Huang et al., 2019), suggesting that the intrusion of western boundary currents not only serves as a net sink of oceanic DOC in marginal seas but also stimulates carbon sequestration through primary production. Possible mechanisms for the impacts of the intrusion of Kuroshio water on biogeochemical processes in the NSCS basin are shown in Fig. 16.11.

16.3.3 Deep layers of the SCS

The deep, dark ocean (i.e., below the photic zone) is the largest reservoir of DOC. This section focuses on the dynamics of DOC in the deep ocean below 100 m in the SCS regions beyond the shelf. It should be noted that available data from the SSCS remain limited to between approximately 11 and 17°N. In the subsurface layer, as shown in Fig. 16.12A, DOC concentrations are generally higher in the NSCS (north of the 17°N) relative to the SSCS at the same σ_θ. Hansell et al. (2012) proposed concentration thresholds for semilabile DOC (SLDOC: >55.6 μmol L^{-1}), semirefractory DOC (SRDOC: 43.8–55.6 μmol L^{-1}), and refractory DOC (RDOC: <43.8 μmol L^{-1}) using data from the North Atlantic. When these thresholds are applied to the SCS, the results indicate that the DOC pool at depths below $\sigma_\theta = 27$ is mainly composed of RDOC, while SLDOC and SRDOC are enriched at potential density range between 22–24 and 24–27, respectively (Fig. 16.12A). Notably, SLDOC and SRDOC are found at deeper potential density layers in the NSCS (as deep as $\sigma_\theta = 26.2$ and 27.6, respectively) compared to in the SSCS (25.1 and 27.2). Apart from including some northern slope stations with higher

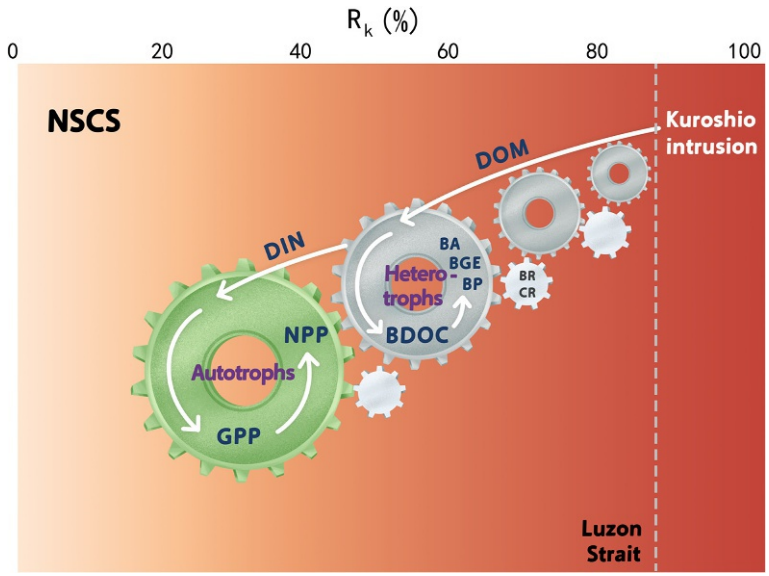

FIG. 16.11 Illustrations of possible mechanisms for the impacts of the Kuroshio intrusion on biogeochemical processes in the NSCS basin. During surface water mass mixing between the Kuroshio and the NSCS, the significant gradient of biogeochemical factors, such as nutrient availability and microbial species, stimulates the decomposition of DOM (such as with the release of ammonium), in turn benefitting autotrophic production. *BA*, bacterial abundance; *BDOC*, biodegradable dissolved organic carbon; *BGE*, bacterial growth efficiency; *BP*, bacterial production; *BR*, bacterial respiration; *CR*, community respiration; *DIN*, dissolved inorganic nitrogen; *DOM*, dissolved organic matter; *GPP*, gross primary production; *NPP*, net primary production; R_k: proportion of Kuroshio water.

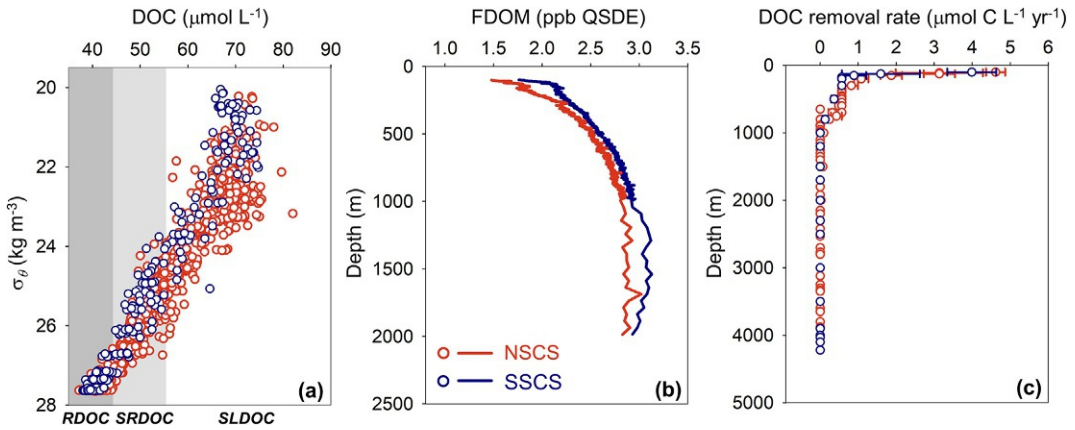

FIG. 16.12 Vertical profiles of (A) dissolved organic carbon (DOC) against potential density (σ_θ), (B) fluorescence intensity of fluorescent dissolved organic matter (FDOM) versus depth, and (C) DOC removal rate versus depth in the SCS. Shaded areas in (A) show concentration thresholds of refractory DOC (RDOC), semirefractory DOC (SRDOC), and semilabile DOC (SLDOC) proposed by Hansell et al. (2012). Data in the NSCS are from Dai et al. (2009), Wu et al. (2015), and Ding et al. (2020); data in the SSCS were collected in May 2014. The average values are plotted for each depth in (B) and (C). Error bars in (C) represent the deviation.

DOC concentrations in the NSCS, the laterally transported organic carbon from the northern margin of the SCS (Shen et al., 2020), where some of the organic carbon can be fresh (Nakatsuka, 2004), is considered the main reason for the difference in DOC distribution between the NSCS and the SSCS basin. The input of fresh organic matter may enhance the remineralization of relatively refractory organic carbon (Bianchi, 2011; Morling et al., 2017), leading to a relatively smaller pool of RDOC. This hypothesis is supported by evidence from optical data collected by Biogeochemical-Argo floats, showing lower fluorescent dissolved organic matter (FDOM) concentrations in the NSCS (1.5–2.9 ppb QSDE in 100–2000 m) compared to the SSCS (1.7–3.1 ppb QSDE; Mann-Whitney U test, $P < .01$; Fig. 16.12B), with FDOM being employed as an indicator for refractory DOM.

Furthermore, when the removal rates of SLDOC, SRDOC, and RDOC estimated from the concentration thresholds and lifetimes of the three DOC pools (Hansell et al., 2012) are applied to the SCS, the results indicate that the bulk DOC removal rate decreases with depth from 4.62 ± 0.25 and $3.99 \pm 0.65\,\mu mol\,C\,L^{-1}\,year^{-1}$ at 100 m to 0.003–0.10 and $0.003\,\mu mol\,C\,L^{-1}\,year^{-1}$ below 1000 m in the NSCS and the SSCS basin, respectively (Fig. 16.12C). Compared to the North Atlantic (NA), the SCS has a lower DOC removal rate at depths between 100 and 200 m ($0.57–4.62\,\mu mol\,C\,L^{-1}\,year^{-1}$ in the SCS; $6.49 \pm 1.44\,\mu mol\,C\,L^{-1}\,year^{-1}$ in the NA, Hansell and Carlson, 2001), but has a similar high-value boundary below 200 m [$0.003–1.08\,\mu mol\,C\,L^{-1}\,year^{-1}$ in the SCS; $0.13–0.96\,\mu mol\,C\,L^{-1}\,year^{-1}$ in the NA (Carlson et al., 2010)]. The DOC removal rate in the SCS below 1000 m ($0.003–0.10\,\mu mol\,C\,L^{-1}\,year^{-1}$) is generally comparable to that in the South Pacific Ocean ($0.004–0.31\,\mu mol\,C\,L^{-1}\,year^{-1}$, Hansell et al. 2012). Compared to other marginal seas, the SCS has a slightly lower average DOC removal rate below 1000 m ($0.01\,\mu mol\,C\,L^{-1}\,year^{-1}$) than in the Japan Sea ($0.04\,\mu mol\,C\,L^{-1}\,year^{-1}$) but is one order of magnitude lower than rates in the Mediterranean Sea ($0.14\,\mu mol\,C\,L^{-1}\,year^{-1}$, Kim et al. 2015). Assuming that DOC removal is solely due to heterotrophic respiration, the DOC pool could potentially supply 1.59 ± 0.06 and $1.05 \pm 0.08\,mmol\,C\,m^{-2}\,day^{-1}$ in the 100–4000 m zone to meet heterotrophic carbon demand in the basin area of NSCS and SSCS, respectively. The heterotrophic carbon demand from the DOC pool is nine- and threefold lower than the supply from the total particulate organic carbon (POC) pool (Shen et al., 2020) in the NSCS basin and the SSCS basin, respectively, even though the SCS DOC pool is much larger than the POC pool (Wu et al., 2015). In addition to biological degradation, processes such as gelation, aggregation, and/or adsorption to particles may also contribute partially to DOC removal.

DOC in the deep ocean is mainly sourced from primary production in the euphotic zone, which exports to depth with overturn of the water column (Hansell et al., 2009). Notably, compared to the wNP, excess DOC was observed in the intermediate layer (~1000–1500 m) of the SCS (Dai et al., 2009; Wu et al., 2015), where the water mass mixing rates are two orders of magnitude higher than rates in the adjacent oceans due to monsoons, typhoons, and strong tides (Wang et al., 2019). A one-dimensional steady-state diffusion advection model constrained by potential temperature indicates net DOC production in the intermediate layer at $\sigma\theta \sim 27.2–27.6$ (~1000–1500 m) in the SCS (Dai et al., 2009). In addition, the regression analysis of ^{14}C-DOC ages versus DOC concentrations indicates enhanced DOC concentrations at water depths below 1500 m (Ding et al., 2022). Net DOC accumulation in the deep SCS, similar to other deep oceans, may be sourced from POC dissolution and

degradation by heterotrophs (Cherrier et al., 1999; Lopez and Hansell, 2021), as well as dark carbon fixation by chemoautotrophic microorganisms (Herndl et al., 2005) such as ammonia-oxidizing archaea (AOA) and nitrite-oxidizing bacteria (NOB) (Zhang et al., 2020). In addition, the SCS is unique in that the net DOC accumulation at depth may be sourced from organic carbon introduced laterally from the margins (Shen et al., 2020). Based on these sources, the excess DOC likely consists mostly of relatively labile DOC, potentially providing carbon to meet heterotrophic microbial carbon demand.

Among these net DOC accumulation processes in the deep ocean, the proportion caused by dark carbon fixation is relatively easy to estimate. The 100–4000 m integrated dark carbon fixation rates measured by the ^{14}C method are 4.1 ± 0.5 mmol C m^{-2} day^{-1} in the NSCS and 1.7 ± 0.1 mmol C m^{-2} day^{-1} in the SSCS basin, which are slightly lower than the export fluxes of POC from the euphotic zone (average across four seasons). The more than two-fold higher dark carbon fixation rate in the NSCS compared to the SSCS basin is consistent with the observed higher ammonium concentrations and chemoautotrophic nitrifier abundances, which may partly result from the remineralization of laterally transported organic matter (Shen et al., 2020). Based on culture experiments with AOA and NOB strains, approximately 5%–15% of fixed carbon can be released in the form of DOC during their growth (Bayer et al., 2023). Therefore, by extrapolating these percentages to the bulk chemoautotrophic microbial community, we estimate that the DOC produced by dark carbon fixation is 0.21 ± 0.03 to 0.72 ± 0.09 mmol C m^{-2} day^{-1} in the NSCS and 0.09 ± 0.01 to 0.30 ± 0.02 mmol C m^{-2} day^{-1} in the SSCS basin. Previous reports indicate that a significant portion of released DOC consists of labile compounds, such as amino acids, thymidine, and B vitamins (Bayer et al., 2019), serving as important carbon sources for heterotrophic activity in the deep ocean.

16.3.4 Microbial contributions to the deep DOC reservoir

Microorganisms play a vital role in the formation of the deep-sea RDOC reservoir. They metabolize labile organic carbon exported from the upper ocean, producing inorganic carbon through respiration while simultaneously synthesizing cell biomass, a process known as secondary production. Heterotrophic bacteria release 1%–9% of their total organic carbon uptake into the DOC reservoir, with biologically resistant DOC accounting for a significant portion of this fraction (Carlson, 2002). Therefore the metabolic activity of heterotrophic prokaryotes is the final factor determining the forms of ocean carbon storage, with prokaryotic production and respiration rates serving as key parameters for assessment.

In the NSCS, heterotrophic prokaryotic production from 0 to 100 m depth was estimated to be 1.1–3.2 mmol C m^{-2} day^{-1} based on the ^{3}H-Leucine incorporation method, while prokaryotic respiration was estimated as 45.6–94.9 mmol C m^{-2} day^{-1} using the INT [2-(4-Iodophenyl)-3-(4-Nitrophenyl)-5-(Phenyl) Tetrazolium Chloride] reduction method (Huang et al., 2019). Prokaryotic growth efficiency (PGE) and carbon demand (PCD) are thus estimated to be 12.7%–24.0% (Huang et al., 2019) and 54.1–96.8 mmol C m^{-2} day^{-1}, respectively, which are higher than those in the adjacent wNP (Shen, 2022). From 100 to 4000 m depth, the integrated heterotrophic prokaryotic production is 2.20 ± 0.15 mmol C m^{-2} day^{-1} in the NSCS and 1.14 ± 0.06 mmol C m^{-2} day^{-1} in the SSCS basin. Based on the average Pacific PGE of 3% (Shen et al., 2020), the PCD is estimated to be 73.30 ± 5.14 mmol C m^{-2} day^{-1} in the NSCS and

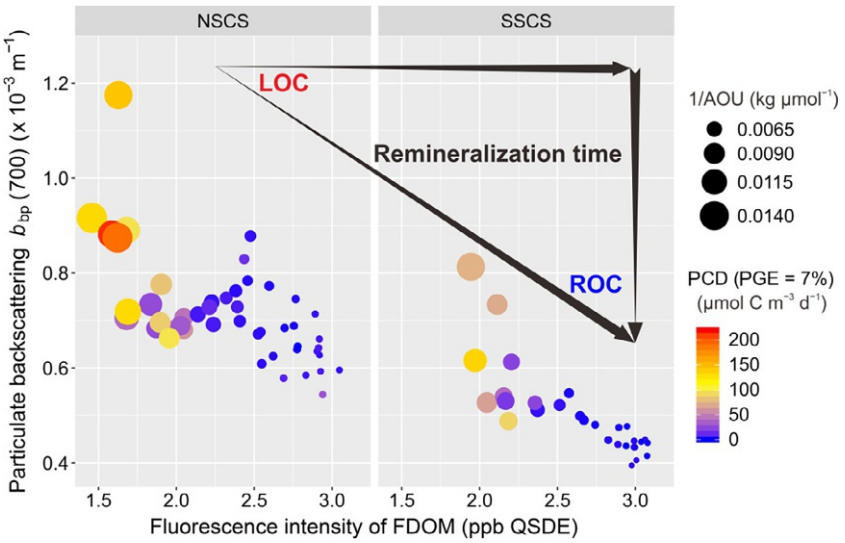

FIG. 16.13 Relationships among prokaryotic carbon demand (PCD), particulate backscattering coefficients (b_{bp}(700)), intensity of fluorescent dissolved organic matter (FDOM), and apparent oxygen utilization (AOU; Spearman, $P < .05$ for each pair). The conceptual diagram in the top right corner, showing decreasing POC and increasing FDOM with remineralization time, suggests labile organic carbon (LOC) degradation and recalcitrant organic carbon (ROC) accumulation in the ocean's interior. *Modified from Shen et al. (2020), with permission from John Wiley & Sons.*

$37.84 \pm 1.90\,\text{mmol C}\,\text{m}^{-2}\,\text{day}^{-1}$ in the SSCS basin, which are also higher than those in the adjacent wNP (Shen, 2022). This outcome suggests that there is relatively more labile organic carbon in the entire water column of the SCS compared to the wNP, reflecting a typical characteristic of marginal seas compared to their adjacent oceans. Moreover, the higher PCD values in the NSCS indicate more labile organic carbon in the NSCS than in the SSCS basin. This enrichment is evidenced by the higher POC (the most important source of labile DOC) and the lower FDOM (a proxy for refractory DOM) in the NSCS than in the SSCS, as well as the significant positive relationship between POC and PCD and the negative relationship between FDOM and PCD (Fig. 16.13).

As described in Section 16.3.3, the total DOC pool from various sources is estimated to supply 1.59 ± 0.06 and $1.05 \pm 0.08\,\text{mmol C}\,\text{m}^{-2}\,\text{day}^{-1}$ of carbon to heterotrophic prokaryotic activity in the 100–4000 m zone of the NSCS and the SSCS basin, respectively. This supply corresponds to approximately 2.2% and 2.8% (based on a PGE of 3%) of total PCD. These proportions are similar to those observed in the meso- and bathypelagic zones of the Atlantic Ocean (1.0%–3.0%, Carlson et al., 2010). It has been suggested that the DOC released by heterotrophic prokaryotes is relatively more refractory than the DOC they take up. Based on estimates of DOC release ranging from 1% to 9% (Carlson, 2002) of total heterotrophic organic carbon uptake (i.e., PCD), heterotrophic prokaryotes in the NSCS and the SSCS basin release approximately $0.73–6.60\,\text{mmol C}\,\text{m}^{-2}\,\text{day}^{-1}$ and $0.38–3.41\,\text{mmol C}\,\text{m}^{-2}\,\text{day}^{-1}$ of DOC into the deep DOC reservoir, respectively. Over time, along with contributions from microbial metabolism occurring across north to south, RDOC accumulates in the southern central basin of the SCS (Figs. 16.12B and 16.13).

16.4 DOC stocks and fluxes

16.4.1 DOC stock in the SCS

We leverage the reconstructed DOC data described in the previous section to estimate DOC stocks and fluxes in the SCS. The mean DOC concentrations were estimated for the four layers of the water column in the SCS, ranging from the euphotic layer (0–100 m) to the deep ocean (>1600 m) using reconstructed data (see Table 16.1). The DOC stock for each layer was then calculated by multiplying the mean DOC concentration by the volume of seawater in that layer. The euphotic layer had the highest mean DOC concentration of $69.7 \pm 5.7\,\mu mol\,L^{-1}$, followed by the mesopelagic and bathypelagic layers with mean DOC concentrations of 50.5 ± 3.9, 44.0 ± 3.2, $41.5 \pm 3.0\,mmol\,L^{-1}$, in the 100–600 m, 600–1600 m, and >1600 m layers, respectively. The higher standard deviations in the euphotic and mesopelagic layers indicate greater spatial variability of DOC in the upper layers than in the deep ocean due to production and consumption processes. The lower DOC concentration variability in the bathypelagic water suggests that it contains less labile fractions of DOC. DOC stocks for the four layers in the SCS were estimated at 218, 548, 750, and 850 Tg C, respectively, totaling 2366 Tg C in the SCS, which accounts for about 0.4% of the global ocean DOC stock of 662 Pg C (Hansell et al., 2009). The estimated DOC stock in the SCS is 1.7 times lower than that reported by Jiao et al. (2018), which is attributable to the larger volume of the deep SCS considered in that study.

16.4.2 Riverine inputs to the SCS

Global assessments of riverine DOC fluxes reveal that 60% of riverine DOC discharges into low-latitude seas (Dai et al., 2012). In Southeast Asia, high precipitation rates facilitate riverine discharge, and changes in land use resulting from high human population densities have caused increasing organic carbon release into freshwater outflows. Huang et al. (2017)

TABLE 16.1 DOC inventories in different layers of the SCS.

Depth layer (m)	Volume ($10^5\,km^3$)[a]	Mean DOC ± SD ($\mu mol\,L^{-1}$)[b]	Stock (10^{12} g C)
0–100	2.62	69.7 ± 5.7	218 ± 18
100–600	9.04	50.5 ± 3.9	548 ± 42
600–1600	14.20	44.0 ± 3.2	750 ± 55
>1600	17.08	41.5 ± 3.0	850 ± 61
Total DOC stock			2366 ± 93

[a] *Seawater volumes are estimated by integrating the SCS topographic data (ETOPO1, Global 1 Arc-minute Ocean Depth and Land Elevation from the US National Geophysical Data Center (NGDC), ds759.4|https://doi.org/10.5065/D69Z92Z5).*

[b] *The average DOC concentration of each water layer was obtained by taking the average value of reconstructed DOC data at the depths in the water layer; the standard deviations of the concentration changes in the vertical direction are included in the table.*

estimated the riverine flux of DOC to the SCS by using previously measured riverine DOC data and reconstructed data in some rivers that lack DOC analysis. The estimated total riverine flux of DOC to the SCS is 25.03 $Tg\,C\,year^{-1}$, which accounts for 30% of the total annual riverine carbon flux to the SCS, including DIC, PIC, and POC fluxes (Huang et al., 2017). Two of the world's largest rivers, the Mekong River ($2.12\,Tg\,DOC\,year^{-1}$) and the Pearl River ($0.71\,Tg\,DOC\,year^{-1}$), along with the other high-discharge rivers ($>1000\,m^3\,s^{-1}$), jointly contribute approximately 75% of the total riverine DOC fluxes (Huang et al., 2017; Liu et al., 2018). The highest DOC flux is estimated in Borneo Bay, which receives river waters high in DOC ($\sim 500\,\mu mol\,L^{-1}$) originating from tropical forests and peatlands in Indonesia (Huang et al., 2017). Considering that the SCS constitutes only 1% of the world's ocean surface area but receives 15% of the global riverine DOC flux ($0.17\,Pg\,C\,year^{-1}$, Dai et al., 2012), we infer a higher riverine input per unit area to the SCS compared to the global average. Previous research has provided evidence of terrestrially and continentally derived organic matter in the particulate phase of the deep SCS (Liu et al., 2007; Blattmann et al., 2019; Zhang et al., 2019). And recent research provided molecular evidence of terrestrial input in the DOC collected from the SCS basin (Jiang et al., 2023). However, the DOC concentrations observed throughout the water column of the SCS basin are similar to that of the Pacific Ocean (Wu et al., 2015; Li et al., 2021). Furthermore, the δ^{13}C-DOC values in the SCS range from −20.5‰ to −23.5‰, consistent with the values reported for DOC in the Pacific Ocean (Zigah et al., 2017; Ding et al., 2020). These observations suggest that additional removal of terrestrial DOC occurs along with the transport and mixing processes in the SCS.

16.4.3 DOC fluxes across the major straits of the SCS

To calculate the fluxes of DOC across the main straits, including the Luzon Strait, the Taiwan Strait, the Karimata Strait, and the Mindoro and Balabac Straits (see Fig. 16.1), the following equation is used:

$$F_c = \overline{\int_0^S (u \times c) ds}$$

where u is the current velocity normal to a given cross-section s, c is the reconstructed DOC concentration, and S is the total integrated length or area. The overbar denotes time averaging. The data source for u is obtained from a previous report (Du et al., 2020). The seasonal and spatial variation in water transport across the four straits may be significantly higher due to the variability of different hydrological situations (Gan et al., 2016; Zheng et al., 2023). The annual mean water transport is applied here to estimate DOC fluxes between the adjacent marginal seas and oceans.

The Luzon Strait serves as the sole deep passage connecting the SCS and the Pacific Ocean, facilitating water exchange and contributing to the unique "sandwich-like" circulation in the SCS (Qu et al., 2006; Gan et al., 2016). The estimated fluxes of DOC in the 0–100 m, 100–600 m, 600–1600 m, and >1600 m layers are 24, 66, −20, and 10 $Tg\,C\,year^{-1}$, respectively (Fig. 16.14).

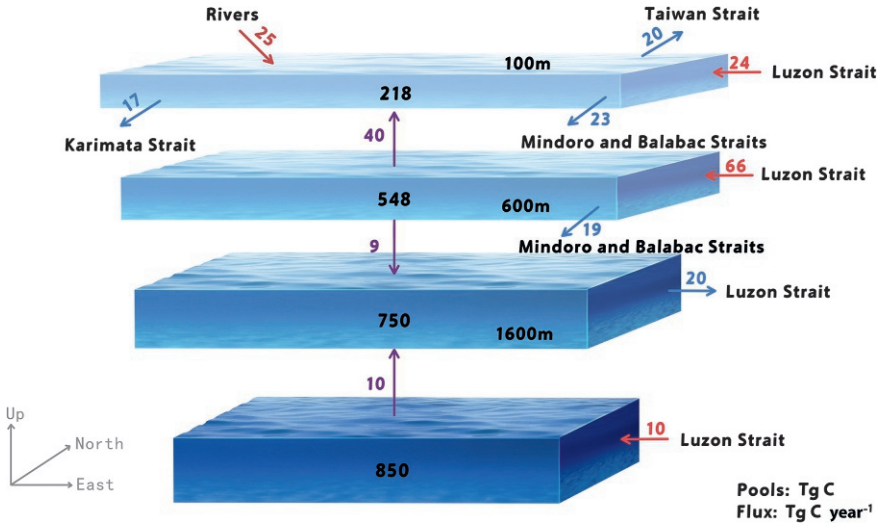

FIG. 16.14 Schematic diagram of DOC transport across the Luzon, Taiwan, Mindoro and Balabac, and Karimata Straits and from rivers in the South China Sea. The *red* and *blue* text and *arrows* denote net influxes and outfluxes (teragrams of carbon per year, Tg C year^{-1}), respectively; the purple text and arrows denote vertical fluxes. Blue values in the boxes indicate DOC reservoirs in teragrams of carbon (Tg C).

The positive and negative values represent the inflow and outflow fluxes, respectively. These estimates are close to estimates obtained from field observations of DOC and water exchange fluxes (107.1, −54.7, and 16.4 Tg C year^{-1}, in the 0–750 m, 750–1500 m, and >1500 m layers, respectively, Wu et al. (2015)). The Kuroshio intrusion contributes exogenous DOC to the surface water of the NSCS, influencing DOC distribution and fueling enhanced microbial activity there (Xu et al., 2018; Huang et al., 2019; Li et al., 2021). Li et al. (2021) estimated that the potential biodegradable carbon and nitrogen from the Kuroshio intrusion added DOC and DON at approximately 8.6 Tg C year^{-1} and 1.2 Tg N year^{-1}, respectively, serving as a critical source of nitrogen that supports production in the NSCS. In the intermediate water layer (1000–1500 m) of the SCS, the DOC level is consistently higher (~2–3 μmol L^{-1}) than in the northwestern Pacific Ocean (Dai et al., 2009; Wu et al., 2017). This excess may result from sinking particle dissolution, lateral particle transport, or stronger vertical mixing of surface DOC. The westward flux of DOC in the middle layer of the SCS could provide a carbon sequestration pathway from the marginal SCS to the interior of the Pacific Ocean. The Taiwan Strait connects the SCS and the ECS, and the estimated annual DOC outflow is −20 Tg C year^{-1} (Fig. 16.14). The Karimata Straits and Mindoro and Balabac Straits connect the SCS to the Indonesian seas (including but not limited to Makassar Strait, Java Sea, Lombok Strait, Flores Sea, Ombai Strait, Timor Sea, Banda Sea, Halmahera Sea, Maluku Sea, Sulawesi Sea), and their transport significantly contributes to the SCS through flow (He et al., 2015). The DOC outflow across the Karimata Strait is −17 Tg C year^{-1}, and the DOC outflow across the Mindoro and Balabac Straits is 42 Tg C year^{-1}, including the fluxes across the upper (0–100 m, 23 Tg C year^{-1}) and intermediate (>100 m, 19 Tg C year^{-1}) layers (Fig. 16.14).

16.5 Summary and perspectives

The SCS, as a mini ocean that experiences dynamic exchanges with both the land and the adjacent oceanic realms, is a natural laboratory for examining intrinsic biogeochemical processes, including the transformation and transportation of DOC under strong influences from the physical environment. On the shelf, DOC inputs are highest from rivers, with enhanced transformation between different DOC pools stimulated by primary production and different microbial processes. In the deep basin, DOC demonstrates distributions and behaviors very similar to other oceanic regimes. Meanwhile, the Kuroshio Current, an important western boundary current, carries oceanic DOC into the SCS through the Luzon Strait, which then exchanges with the North Pacific and Indonesian seas. The horizontal transport of labile DOC sustains microbial activity in the SCS and neighboring regions. The SCS is also a conduit for the export of DOC into the interiors of the open ocean in support of deep, dark ocean microbiomes, highlighting the vital role of SCS DOC in the regional and global carbon cycle.

Acknowledgments

This project was supported by NSFC grants #42188102 (to MD), #42276034 (to XL), and #42125603 (to YZ). We thank the National Basic Research Program of China (973 Program), the Ministry of Science and Technology, and the National Science Foundation of China (NSFC) for their sustained support of biogeochemical research in the South China Sea and adjacent North Pacific Ocean over the past two decades. We are indebted to the numerous students, postdoctoral scientists, and technicians who have contributed to our research programs over the years, including but not limited to Jianrong Lin, Kai Wu, Shuai Gu, Peng Jiang, Jiaming Shen, Xi Dai, Tiantian Tang, and Junhui Chen. We acknowledge Chuanjun Du and Xiaolong Yu for providing the modeled current velocity in the South China Sea and the depth of the euphotic zone at the Southeast Asian Time-series Study (SEATS) station.

References

Adamson, P.T., Rutherfurd, I.D., Peel, M.C., Conlan, I.A., 2009. The hydrology of the Mekong river. In: Campbell, I.C. (Ed.), The Mekong. Academic Press, Cambridge, pp. 53–76 (Chapter 4).

Bauer, J.E., Cai, W.-J., Raymond, P.A., Bianchi, T.S., Hopkinson, C.S., Regnier, P.A.G., 2013. The changing carbon cycle of the coastal ocean. Nature 504, 61–70. https://doi.org/10.1038/nature12857.

Bayer, B., Hansman, R.L., Bittner, M.J., Noriega-Ortega, B.E., Niggemann, J., Dittmar, T., Herndl, G.J., 2019. Ammonia-oxidizing archaea release a suite of organic compounds potentially fueling prokaryotic heterotrophy in the ocean. Environ. Microbiol. 21 (11), 4062–4075. https://doi.org/10.1111/1462-2920.14755.

Bayer, B., McBeain, K., Carlson, C.A., Santoro, A.E., 2023. Carbon content, carbon fixation yield and dissolved organic carbon release from diverse marine nitrifiers. Limnol. Oceanogr. 68 (1), 84–96. https://doi.org/10.1002/lno.12252.

Bianchi, T.S., 2011. The role of terrestrially derived organic carbon in the coastal ocean: a changing paradigm and the priming effect. Proc. Natl. Acad. Sci. USA 108 (49), 19473–19481. https://doi.org/10.1073/pnas.1017982108.

Blattmann, T.M., Liu, Z., Zhang, Y., Zhao, Y., Haghipour, N., Montlucon, D.B., Plotze, M., Eglinton, T.I., 2019. Mineralogical control on the fate of continentally derived organic matter in the ocean. Science 366 (6466), 742–745. https://doi.org/10.1126/science.aax5345.

Broecker, W.S., Patzert, W.C., Toggweiler, J.R., Stuiver, M., 1986. Hydrography, chemistry, and radioisotopes in the Southeast Asian basins. J. Geophys. Res. 91 (C12). https://doi.org/10.1029/JC091iC12p14345.

Callahan, J., Dai, M., Chen, R.F., Li, X., Lu, Z., Huang, W., 2004. Distribution of dissolved organic matter in the Pearl River Estuary, China. Mar. Chem. 89 (1-4), 211–224. https://doi.org/10.1016/j.marchem.2004.02.013.

Cao, Z., Dai, M., 2011. Shallow-depth $CaCO_3$ dissolution: Evidence from excess calcium in the South China Sea and its export to the Pacific Ocean. Global Biogeochem. Cycles 25 (2), GB2019. https://doi.org/10.1029/2009gb003690.

Cao, Z., Dai, M., Zheng, N., Wang, D., Li, Q., Zhai, W., Meng, F., Gan, J., 2011. Dynamics of the carbonate system in a large continental shelf system under the influence of both a river plume and coastal upwelling. J. Geophys. Res. 116 (G2). https://doi.org/10.1029/2010jg001596.

Cao, Z., Yang, W., Zhao, Y., Guo, X., Yin, Z., Du, C., Zhao, H., Dai, M., 2020. Diagnosis of CO_2 dynamics and fluxes in global coastal oceans. Natl. Sci. Rev. 7 (4), 786–797.

Carlson, C.A., 2002. Production and removal processes. In: Carlson, C.A., Hansell, D.A. (Eds.), Biogeochemistry of Marine Dissolved Organic Matter. Academic Press, San Diego, CA, pp. 91–151.

Carlson, C.A., Ducklow, H.W., Michaels, A.F., 1994. Annual flux of dissolved organic carbon from the euphotic zone in the northwestern Sargasso Sea. Nature 371 (6496), 405–408. https://doi.org/10.1038/371405a0.

Carlson, C.A., Giovannoni, S.J., Hansell, D.A., Goldberg, S.J., Parsons, R., Vergin, K., 2004. Interactions among dissolved organic carbon, microbial processes, and community structure in the mesopelagic zone of the northwestern Sargasso Sea. Limnol. Oceanogr. 49 (4), 1073–1083. https://doi.org/10.4319/lo.2004.49.4.1073.

Carlson, C.A., Hansell, D.A., Nelson, N.B., Siegel, D.A., Smethie, W.M., Khatiwala, S., Meyers, M.M., Halewood, E., 2010. Dissolved organic carbon export and subsequent remineralization in the mesopelagic and bathypelagic realms of the North Atlantic basin. Deep-Sea Res. II 57 (16), 1433–1445. https://doi.org/10.1016/j.dsr2.2010.02.013.

Chen, W., Liu, Q., Huh, C.A., Dai, M., Miao, Y.C., 2010. Signature of the Mekong river plume in the western South China Sea revealed by radium isotopes. J. Geophys. Res. Oceans 115 (C12). https://doi.org/10.1029/2010JC006460.

Cherrier, J., Bauer, J.E., Druffel, E.R.M., Coffin, R.B., Chanton, J.P., 1999. Radiocarbon in marine bacteria: evidence for the ages of assimilated carbon. Limnol. Oceanogr. 44 (3), 730–736. https://doi.org/10.4319/lo.1999.44.3.0730.

Chou, W.-C., Chen, Y.-L.L., Sheu, D.D., Shih, Y.-Y., Han, C.-A., Cho, C.L., Tseng, C.-M., Yang, Y.-J., 2006. Estimated net community production during the summertime at the SEATS time-series study site, northern South China Sea: implications for nitrogen fixation. Geophys. Res. Lett. 33 (22). https://doi.org/10.1029/2005gl025365.

Chou, W.C., Sheu, D.D., Lee, B.S., Tseng, C.M., Chen, C.T.A., Wang, S.L., Wong, G.T.F., 2007. Depth distributions of alkalinity, TCO_2 and at SEATS time-series site in the northern South China Sea. Deep-Sea Res. II 54 (14-15), 1469–1485. https://doi.org/10.1016/j.dsr2.2007.05.002.

Dai, M., Meng, F., Tang, T., Kao, S.-J., Lin, J., Chen, J., Huang, J.-C., Tian, J., Gan, J., Yang, S., 2009. Excess total organic carbon in the intermediate water of the South China Sea and its export to the North Pacific. Geochem. Geophys. Geosyst. 10 (12). https://doi.org/10.1029/2009GC002752.

Dai, M., Yin, Z., Meng, F., Liu, Q., Cai, W.-J., 2012. Spatial distribution of riverine DOC inputs to the ocean: an updated global synthesis. Curr. Opin. Environ. Sustain. 4 (2), 170–178. https://doi.org/10.1016/j.cosust.2012.03.003.

Dai, M., Cao, Z., Guo, X., Zhai, W., Liu, Z., Yin, Z., Xu, Y., Gan, J., Hu, J., Du, C., 2013. Why are some marginal seas sources of atmospheric CO_2? Geophys. Res. Lett. 40 (10), 2154–2158. https://doi.org/10.1002/grl.50390.

Dai, M., Gan, J., Han, A., Kung, H., Yin, Z., 2014. Physical dynamics and biogeochemistry of the Pearl River plume. In: Bianchi, T., Allison, M., Cai, W.-J. (Eds.), Biogeochemical Dynamics at Major River-Coastal Interfaces: Linkages with Global Change. Cambridge University Press, Cambridge, pp. 321–352.

Dai, M., Su, J., Zhao, Y., Hofmann, E.E., Cao, Z., Cai, W.-J., Gan, J., Lacroix, F., Laruelle, G.G., Meng, F., Müller, J.D., Regnier, P.A.G., Wang, G., Wang, Z., 2022. Carbon fluxes in the coastal ocean: synthesis, boundary processes, and future trends. Annu. Rev. Earth Planet. Sci. 50 (1), 593–626. https://doi.org/10.1146/annurev-earth-032320-090746.

Dai, M., Zhao, Y., Chai, F., Chen, M., Chen, N., Chen, Y., Cheng, D., Gan, J., Guan, D., Hong, Y., Huang, J., Lee, Y., Leung, K.M.Y., Lim, P.E., Lin, S., Lin, X., Liu, X., Liu, Z., Luo, Y.-W., Meng, F., Sangmanee, C., Shen, Y., Uthaipan, K., Wan Talaat, W.I.A., Wan, X.S., Wang, C., Wang, D., Wang, G., Wang, S., Wang, Y., Wang, Y., Wang, Z., Wang, Z., Xu, Y., Yang, J.-Y.T., Yang, Y., Yasuhara, M., Yu, D., Yu, J., Yu, L., Zhang, Z., Zhang, Z., 2023. Persistent eutrophication and hypoxia in the coastal ocean. Camb. Prism. Coast. Futur. 1, e19. https://doi.org/10.1017/cft.2023.7.

Ding, L., Qi, Y., Shan, S., Ge, T., Luo, C., Wang, X., 2020. Radiocarbon in dissolved organic and inorganic carbon of the South China Sea. J. Geophys. Res. Oceans 125 (4). https://doi.org/10.1029/2020jc016073.

Ding, L., Shan, S., Luo, C., Wang, X., 2022. Distribution and microbial degradation of dissolved organic carbon in the northern South China Sea. Front. Mar. Sci. 9. https://doi.org/10.3389/fmars.2022.973694.

Du, C., Liu, Z., Dai, M., Kao, S.J., Cao, Z., Zhang, Y., Huang, T., Wang, L., Li, Y., 2013. Impact of the Kuroshio intrusion on the nutrient inventory in the upper northern South China Sea: insights from an isopycnal mixing model. Biogeosciences 10 (10), 6419–6432. https://doi.org/10.5194/bg-10-6419-2013.

Du, C., Liu, Z., Kao, S.J., Dai, M., 2017. Diapycnal fluxes of nutrients in an oligotrophic oceanic regime: the South China Sea. Geophys. Res. Lett. 44 (22), 11510–11518. https://doi.org/10.1002/2017gl074921.

Du, C., Gan, J., Hui, C.R., Lu, Z., Zhao, X., Roberts, E., Dai, M., 2020. Dynamics of dissolved inorganic carbon in the South China Sea: a modeling study. Prog. Oceanogr. 186. https://doi.org/10.1016/j.pocean.2020.102367.

Du, C., He, R., Liu, Z., Huang, T., Wang, L., Yuan, Z., Xu, Y., Wang, Z., Dai, M., 2021. Climatology of nutrient distributions in the South China Sea based on a large data set derived from a new algorithm. Prog. Oceanogr. 195. https://doi.org/10.1016/j.pocean.2021.102586.

Furue, R., Yu, Z., McCreary, J., Yaremchuk, M., 2009. The South China Sea through flow retrieved from climatological data. J. Phys. Oceanogr. 39 (3), 753–767. https://doi.org/10.1175/2008jpo3955.1.

Gan, J., Liu, Z., Hui, C.R., 2016. A three-layer alternating spinning circulation in the South China Sea. J. Phys. Oceanogr. 46 (8), 2309–2315. https://doi.org/10.1175/Jpo-D-16-0044.1.

Han, A., Dai, M., Kao, S.-J., Gan, J., Li, Q., Wang, L., Zhai, W., Wang, L., 2012. Nutrient dynamics and biological consumption in a large continental shelf system under the influence of both a river plume and coastal upwelling. Limnol. Oceanogr. 57 (2), 486–502. https://doi.org/10.4319/lo.2012.57.2.0486.

Han, A.Q., Dai, M.H., Gan, J.P., Kao, S.J., Zhao, X.Z., Jan, S., Li, Q., Lin, H., Chen, C.T.A., Wang, L., Hu, J.Y., Wang, L.F., Gong, F., 2013. Inter-shelf nutrient transport from the East China Sea as a major nutrient source supporting winter primary production on the northeast South China Sea shelf. Biogeosciences 10 (12), 8159–8170. https://doi.org/10.5194/bg-10-8159-2013.

Hanebuth, T.J.J., Voris, H.K., Yokoyama, Y., Saito, Y., Okuno, J.I., 2011. Formation and fate of sedimentary depocentres on Southeast Asia's Sunda Shelf over the past sea-level cycle and biogeographic implications. Earth Sci. Rev. 104 (1-3), 92–110. https://doi.org/10.1016/j.earscirev.2010.09.006.

Hansell, D.A., Carlson, C.A., 1998. Net community production of dissolved organic carbon. Global Biogeochem. Cycles 12 (3), 443–453. https://doi.org/10.1029/98gb01928.

Hansell, D.A., Carlson, C.A., 2001. Biogeochemistry of total organic carbon and nitrogen in the Sargasso Sea: control by convective overturn. Deep-Sea Res. II 48 (8-9), 1649–1667. https://doi.org/10.1016/s0967-0645(00)00153-3.

Hansell, D.A., Carlson, C.A., Suzuki, Y., 2002. Dissolved organic carbon export with North Pacific intermediate water formation. Global Biogeochem. Cycles 16 (1), 7-1–7-8. https://doi.org/10.1029/2000gb001361.

Hansell, D., Carlson, C., Repeta, D., Schlitzer, R., 2009. Dissolved organic matter in the ocean: a controversy stimulates new insights. Oceanography 22 (4), 202–211. https://doi.org/10.5670/oceanog.2009.109.

Hansell, D.A., Carlson, C.A., Schlitzer, R., 2012. Net removal of major marine dissolved organic carbon fractions in the subsurface ocean. Global Biogeochem. Cycles 26 (1), GB1016. https://doi.org/10.1029/2011gb004069.

He, B., Dai, M., Zhai, W., Wang, L., Wang, K., Chen, J., Lin, J., Han, A., Xu, Y., 2010. Distribution, degradation and dynamics of dissolved organic carbon and its major compound classes in the Pearl River estuary, China. Mar. Chem. 119 (1-4), 52–64. https://doi.org/10.1016/j.marchem.2009.12.006.

He, Z., Feng, M., Wang, D., Slawinski, D., 2015. Contribution of the Karimata Strait transport to the Indonesian throughflow as seen from a data assimilation model. Cont. Shelf Res. 92, 16–22. https://doi.org/10.1016/j.csr.2014.10.007.

Herndl, G.J., Reinthaler, T., Teira, E., van Aken, H., Veth, C., Pernthaler, A., Pernthaler, J., 2005. Contribution of Archaea to total prokaryotic production in the deep Atlantic Ocean. Appl. Environ. Microbiol. 71 (5), 2303–2309. https://doi.org/10.1128/AEM.71.5.2303-2309.2005.

Hu, J., Wang, X.H., 2016. Progress on upwelling studies in the China seas. Rev. Geophys. 54 (3), 653–673. https://doi.org/10.1002/2015rg000505.

Huang, T.H., Chen, C.T.A., Tseng, H.C., Lou, J.Y., Wang, S.L., Yang, L., Kandasamy, S., Gao, X., Wang, J.T., Aldrian, E., Jacinto, G.S., Anshari, G.Z., Sompongchaiyakul, P., Wang, B.J., 2017. Riverine carbon fluxes to the South China Sea. J. Geophys. Res. Biogeosci. 122 (5), 1239–1259. https://doi.org/10.1002/2016jg003701.

Huang, Y., Laws, E., Chen, B., Huang, B., 2019. Stimulation of heterotrophic and autotrophic metabolism in the mixing zone of the kuroshio current and Northern South China Sea: implications for export production. J. Geophys. Res. Biogeosci. 124 (9), 2645–2661. https://doi.org/10.1029/2018jg004833.

Jiang, P., Chen, H., Liu, Z., Li, X., 2023. Comparing the isotopic and molecular composition of dissolved organic carbon between the oligotrophic South China Sea and the adjacent North Pacific Ocean: signals of biodegradation, conservative mixing, and terrestrial input. Mar. Chem. 257 (2023), 104331. https://doi.org/10.1016/j.marchem.2023.104331.

Jiao, N., Liang, Y., Zhang, Y., Liu, J., Zhang, Y., Zhang, R., Zhao, M., Dai, M., Zhai, W., Gao, K., Song, J., Yuan, D., Li, C., Lin, G., Huang, X., Yan, H., Hu, L., Zhang, Z., Wang, L., Cao, C., Luo, Y., Luo, T., Wang, N., Dang, H., Wang, D.,

Zhang, S., 2018. Carbon pools and fluxes in the China seas and adjacent oceans. Sci. China Earth Sci. 61 (11), 1535–1563. https://doi.org/10.1007/s11430-018-9190-x.
Kao, S.-J., Shiah, F.-K., Wang, C.-H., Liu, K.-K., 2006. Efficient trapping of organic carbon in sediments on the continental margin with high fluvial sediment input off southwestern Taiwan. Cont. Shelf Res. 26 (20), 2520–2537. https://doi.org/10.1016/j.csr.2006.07.030.
Kao, S.-J., Terence Yang, J.-Y., Liu, K.-K., Dai, M., Chou, W.-C., Lin, H.-L., Ren, H., 2012. Isotope constraints on particulate nitrogen source and dynamics in the upper water column of the oligotrophic South China Sea. Global Biogeochem. Cycles 26 (2), GB2033. https://doi.org/10.1029/2011gb004091.
Kim, T.H., Kim, G., Lee, S.A., Dittmar, T., 2015. Extraordinary slow degradation of dissolved organic carbon (DOC) in a cold marginal sea. Sci. Rep. 5, 13808. https://doi.org/10.1038/srep13808.
Li, X., Liu, Z., Chen, W., Wang, L., He, B., Wu, K., Gu, S., Jiang, P., Huang, B., Dai, M., 2018. Production and transformation of dissolved and particulate organic matter as indicated by amino acids in the Pearl River Estuary, China. J. Geophys. Res. Biogeosci. 123, 3523–3537.
Li, X., Wu, K., Gu, S., Jiang, P., Li, H., Liu, Z., Dai, M., 2021. Enhanced biodegradation of dissolved organic carbon in the western boundary Kuroshio current when intruded to the marginal South China Sea. J. Geophys. Res.-Oceans 126 (11). https://doi.org/10.1029/2021JC017585.
Liu, Z., Gan, J., 2017. Three-dimensional pathways of water masses in the South China Sea: a modeling study. J. Geophys. Res. Oceans 122 (7), 6039–6054. https://doi.org/10.1002/2016jc012511.
Liu, K.-K., Kao, S.-J., Hu, H.-C., Chou, W.-C., Hung, G.-W., Tseng, C.-M., 2007. Carbon isotopic composition of suspended and sinking particulate organic matter in the northern South China Sea—from production to deposition. Deep-Sea Res. II 54 (14-15), 1504–1527. https://doi.org/10.1016/j.dsr2.2007.05.010.
Liu, K.-K., Atkinson, L., Quiñones, R., Talaue-McManus, L., 2010. Carbon and Nutrient Fluxes in Continental Margins. Springer, Berlin, p. 741.
Liu, K.-K., Wang, L.W., Dai, M., Tseng, C.M., Yang, Y., Sui, C.H., Oey, L., Tseng, K.Y., Huang, S.M., 2013. Inter-annual variation of chlorophyll in the northern South China Sea observed at the SEATS Station and its asymmetric responses to climate oscillation. Biogeosciences 10 (11), 7449–7462. https://doi.org/10.5194/bg-10-7449-2013.
Liu, Q., Guo, X., Yin, Z., Zhou, K., Roberts, E.G., Dai, M., 2018. Carbon fluxes in the China Seas: an overview and perspective. Sci. China Earth Sci. 61 (11), 1564–1582. https://doi.org/10.1007/s11430-017-9267-4.
Lopez, C.N., Hansell, D.A., 2021. Evidence of deep DOC enrichment via particle export beneath subarctic and northern subtropical fronts in the North Pacific. Front. Mar. Sci. 8, 659034. https://doi.org/10.3389/fmars.2021.659034.
Lu, Z., Gan, J., Dai, M., Liu, H., Zhao, X., 2018. Joint effects of extrinsic biophysical fluxes and intrinsic hydrodynamics on the formation of hypoxia west off the Pearl river estuary. J. Geophys. Res. Oceans 123 (9), 6241–6259. https://doi.org/10.1029/2018jc014199.
Lu, Z., Gan, J., Dai, M., Zhao, X., Hui, C.R., 2020. Nutrient transport and dynamics in the South China Sea: a modeling study. Prog. Oceanogr. 183. https://doi.org/10.1016/j.pocean.2020.102308.
Ma, W., Xiu, P., Yu, Y., Zheng, Y., Chai, F., 2021. Production of dissolved organic carbon in the South China Sea: a modeling study. Sci. China Earth Sci. 65 (2), 351–364. https://doi.org/10.1007/s11430-021-9817-2.
Meng, F., Dai, M., Cao, Z., Wu, K., Zhao, X., Li, X., Chen, J., Gan, J., 2017. Seasonal dynamics of dissolved organic carbon under complex circulation schemes on a large continental shelf: the Northern South China Sea. J. Geophys. Res.-Oceans 122 (12), 9415–9428. https://doi.org/10.1002/2017jc013325.
Morling, K., Raeke, J., Kamjunke, N., Reemtsma, T., Tittel, J., 2017. Tracing aquatic priming effect during microbial decomposition of terrestrial dissolved organic carbon in chemostat experiments. Microb. Ecol. 74 (3), 534–549. https://doi.org/10.1007/s00248-017-0976-0.
Nakatsuka, T., 2004. Dissolved and particulate organic carbon in the Sea of Okhotsk: transport from continental shelf to ocean interior. J. Geophys. Res. 109 (C9). https://doi.org/10.1029/2003jc001909.
Nan, F., Xue, H., Yu, F., 2015. Kuroshio intrusion into the South China Sea: a review. Prog. Oceanogr. 137, 314–333. https://doi.org/10.1016/j.pocean.2014.05.012.
Pan, X., Achterberg, E.P., Sanders, R., Poulton, A.J., Oliver, K.I.C., Robinson, C., 2014. Dissolved organic carbon and apparent oxygen utilization in the Atlantic Ocean. Deep Sea Res. I Oceanogr. Res. Pap. 85, 80–87. https://doi.org/10.1016/j.dsr.2013.12.003.
Qu, T., Mitsudera, H., Yamagata, T., 2000. Intrusion of the North Pacific waters into the South China Sea. J. Geophys. Res.-Oceans 105 (C3), 6415–6424. https://doi.org/10.1029/1999jc900323.
Qu, T., Girton, J.B., Whitehead, J.A., 2006. Deepwater overflow through Luzon Strait. J. Geophys. Res. 111 (C1). https://doi.org/10.1029/2005jc003139.

Shen, J., 2022. Research on Carbon Supply and Microbial Carbon Demand in the Dark Ocean of the South China Sea. PhD thesis in Chinese, Xiamen University.

Shen, Y., Fichot, C.G., Benner, R., 2012. Dissolved organic matter composition and bioavailability reflect ecosystem productivity in the Western Arctic Ocean. Biogeosciences 9 (12), 4993–5005. https://doi.org/10.5194/bg-9-4993-2012.

Shen, J., Jiao, N., Dai, M., Wang, H., Qiu, G., Chen, J., Li, H., Kao, S.-J., Yang, J.Y.T., Cai, P., Zhou, K., Yang, W., Zhu, Y., Liu, Z., Chen, M., Zuo, Z., Gaye, B., Wiesner, M.G., Zhang, Y., 2020. Laterally transported particles from margins serve as a major carbon and energy source for dark ocean ecosystems. Geophys. Res. Lett. 47 (18). https://doi.org/10.1029/2020gl088971.

Sheu, D.D., Chou, W.C., Wei, C.L., Hou, W.P., Wong, G.T.F., Hsu, C.W., 2010. Influence of El Niño on the sea-to-air CO_2 flux at the SEATS time-series site, northern South China Sea. J. Geophys. Res. Oceans 115 (C10). https://doi.org/10.1029/2009jc006013.

Shiah, F.K., Kao, S.-J., Liu, K.-K., 1998. Bacterial production in the western equatorial Pacific: implications of inorganic nutrient effects on dissolved organic carbon accumulation and consumption. Bull. Mar. Sci. 63, 795–808.

Song, X., Lai, Z., Ji, R., Chen, C., Zhang, J., Huang, L., Yin, J., Wang, Y., Lian, S., Zhu, X., 2012. Summertime primary production in northwest South China Sea: interaction of coastal eddy, upwelling and biological processes. Cont. Shelf Res. 48, 110–121. https://doi.org/10.1016/j.csr.2012.07.016.

Stadnyk, T.A., Tefs, A., Broesky, M., Déry, S.J., Myers, P.G., Ridenour, N.A., Koenig, K., Vonderbank, L., Gustafsson, D., 2021. Changing freshwater contributions to the Arctic: a 90-year trend analysis (1981–2070). Elementa: Sci. Anthrop. 9 (1). https://doi.org/10.1525/elementa.2020.00098.

Syvitski, J.P., Vorosmarty, C.J., Kettner, A.J., Green, P., 2005. Impact of humans on the flux of terrestrial sediment to the global coastal ocean. Science 308 (5720), 376–380. https://doi.org/10.1126/science.1109454.

Tian, J., Yang, Q., Liang, X., Xie, L., Hu, D., Wang, F., Qu, T., 2006. Observation of Luzon Strait transport. Geophys. Res. Lett. 33 (19). https://doi.org/10.1029/2006GL026272.

Tian, J., Yang, Q., Zhao, W., 2009. Enhanced diapycnal mixing in the South China Sea. J. Phys. Oceanogr. 39 (12), 3191–3203. https://doi.org/10.1175/2009jpo3899.1.

Tseng, C.M., Wong, G.T.F., Lin, I.I., Wu, C.R., Liu, K.K., 2005. A unique seasonal pattern in phytoplankton biomass in low-latitude waters in the South China Sea. Geophys. Res. Lett. 32 (8). https://doi.org/10.1029/2004gl022111.

Tseng, C.M., Wong, G.T.F., Chou, W.C., Lee, B.S., Sheu, D.D., Liu, K.K., 2007. Temporal variations in the carbonate system in the upper layer at the SEATS station. Deep-Sea Res. II 54 (14-15), 1448–1468. https://doi.org/10.1016/j.dsr2.2007.05.003.

Wang, D., Wang, Q., Cai, S., Shang, X., Peng, S., Shu, Y., Xiao, J., Xie, X., Zhang, Z., Liu, Z., Lan, J., Chen, D., Xue, H., Wang, G., Gan, J., Xie, X., Zhang, R., Chen, H., Yang, Q., 2019. Advances in research of the mid-deep South China Sea circulation. Sci. China Earth Sci. 62 (12), 1992–2004. https://doi.org/10.1007/s11430-019-9546-3.

Wong, G.T.F., Ku, T.-L., Mulholland, M., Tseng, C.-M., Wang, D.-P., 2007. The SouthEast Asian Time-series Study (SEATS) and the biogeochemistry of the South China Sea—an overview. Deep-Sea Res. II 54 (14-15), 1434–1447. https://doi.org/10.1016/j.dsr2.2007.05.012.

Wu, J., Chung, S.-W., Wen, L.-S., Liu, K.-K., Chen, Y.-L.L., Chen, H.-Y., Karl, D.M., 2003. Dissolved inorganic phosphorus, dissolved iron, and Trichodesmium in the oligotrophic South China Sea. Global Biogeochem. Cycles 17 (1), 8-1–8-10. https://doi.org/10.1029/2002gb001924.

Wu, K., Dai, M., Chen, J., Meng, F., Li, X., Liu, Z., Du, C., Gan, J., 2015. Dissolved organic carbon in the South China Sea and its exchange with the Western Pacific Ocean. Deep-Sea Res. II 122, 41–51. https://doi.org/10.1016/j.dsr2.2015.06.013.

Wu, K., Dai, M., Li, X., Meng, F., Chen, J., Lin, J., 2017. Dynamics and production of dissolved organic carbon in a large continental shelf system under the influence of both river plume and coastal upwelling. Limnol. Oceanogr. 62 (3), 973–988. https://doi.org/10.1002/lno.10479.

Wyrtki, K., 1961. Physical Oceanography of the Southeast Asian Waters. Library—Scripps Digital Collection, UC San Diego. Retrieved from https://escholarship.org/uc/item/49n9x3t4.

Xiu, P., Dai, M., Chai, F., Zhou, K., Zeng, L., Du, C., 2018. On contributions by wind-induced mixing and eddy pumping to interannual chlorophyll variability during different ENSO phases in the northern South China Sea. Limnol. Oceanogr. 64 (2), 503–514. https://doi.org/10.1002/lno.11055.

Xiu, P., Dai, M., Chai, F., Zhou, K., Zeng, L., Du, C., 2019. On contributions by wind-induced mixing and eddy pumping to interannual chlorophyll variability during different ENSO phases in the northern South China Sea. Limnol. Oceanogr. 64 (2), 503–514. https://doi.org/10.1002/lno.11055.

Xu, M.N., Zhang, W., Zhu, Y., Liu, L., Zheng, Z., Wan, X.S., Qian, W., Dai, M., Gan, J., Hutchins, D.A., Kao, S.-J., 2018. Enhanced ammonia oxidation caused by lateral kuroshio intrusion in the boundary zone of the Northern South China Sea. Geophys. Res. Lett. 45 (13), 6585–6593. https://doi.org/10.1029/2018gl077896.

Zhang, J., Li, H., Xuan, J., Wu, Z., Yang, Z., Wiesner, M.G., Chen, J., 2019. Enhancement of mesopelagic sinking particle fluxes due to upwelling, aerosol deposition, and monsoonal influences in the Northwestern South China Sea. J. Geophys. Res. Oceans 124 (1), 99–112. https://doi.org/10.1029/2018jc014704.

Zhang, Y., Qin, W., Hou, L., Zakem, E.J., Wan, X., Zhao, Z., Liu, L., Hunt, K.A., Jiao, N., Kao, S.J., Tang, K., Xie, X., Shen, J., Li, Y., Chen, M., Dai, X., Liu, C., Deng, W., Dai, M., Ingalls, A.E., Stahl, D.A., Herndl, G.J., 2020. Nitrifier adaptation to low energy flux controls inventory of reduced nitrogen in the dark ocean. Proc. Natl. Acad. Sci. USA 117 (9), 4823–4830. https://doi.org/10.1073/pnas.1912367117.

Zhao, H., Dai, M., Gan, J., Zhao, X., Lu, Z., Liang, L., Liu, Z., Su, J., Cao, Z., 2021. River-dominated pCO_2 dynamics in the northern South China Sea during summer: a modeling study. Prog. Oceanogr. 190. https://doi.org/10.1016/j.pocean.2020.102457.

Zheng, Q., Hu, J., Ho, C.-R., Xie, L., 2020. Advances in research of regional oceanography of the South China Sea: overview. In: Regional Oceanography of the South China Sea. World Scientific Publishing Company, Singapore, pp. 1–18.

Zheng, Y., Ma, W., Wang, Y., Liu, Z., Xiu, P., 2023. Modeling dissolved organic carbon exchange across major straits and shelf breaks in the South China Sea. Prog. Oceanogr. 210. https://doi.org/10.1016/j.pocean.2022.102928.

Zhou, K., Dai, M., Maiti, K., Chen, W., Chen, J., Hong, Q., Ma, Y., Xiu, P., Wang, L., Xie, Y., 2020. Impact of physical and biogeochemical forcing on particle export in the South China Sea. Prog. Oceanogr. 187. https://doi.org/10.1016/j.pocean.2020.102403.

Zhu, Y., Liu, J., Mulholland, M.R., Du, C., Wang, L., Widner, B., Huang, T., Yang, Y., Dai, M., 2021. Dynamics of ammonium biogeochemistry in an oligotrophic regime in the South China Sea. Mar. Chem. 237. https://doi.org/10.1016/j.marchem.2021.104040.

Zigah, P.K., McNichol, A.P., Xu, L., Johnson, C., Santinelli, C., Karl, D.M., Repeta, D.J., 2017. Allochthonous sources and dynamic cycling of ocean dissolved organic carbon revealed by carbon isotopes. Geophys. Res. Lett. 44 (5), 2407–2415. https://doi.org/10.1002/2016gl071348.

Glossary

OceMar ocean-dominated margin, in contrast to RiOMar, is characterized by concurrent off-site inputs, typically from depth, of nutrients and dissolved inorganic carbon (DIC). These materials are upwelled or mixed into the euphotic zone, where nutrients support enhanced primary production to consume DIC. Changes in DIC relative to nutrients, both transformed by physical transport and biological processes, determine the OceMar as a source or sink of atmospheric CO_2.

RiOMar river-dominated Ocean margin is featured by concurrent inputs of autotrophic (nutrients) and heterotrophic (organic matter) loadings from terrestrial sources at the surface. The interplay of these two inputs largely determines the RiOmar as a source or sink of atmospheric CO_2.

This page intentionally left blank